

**RETRIEVAL OF OPTICAL AND MICROPHYSICAL PROPERTIES
OF ICE CLOUDS USING ATMOSPHERIC RADIATION
MEASUREMENT (ARM) DATA**

A Thesis

by

JACQUELINE ANNE KINNEY

Submitted to the Office of Graduate Studies of
Texas A&M University
in partial fulfillment of the requirements for the degree of

MASTER OF SCIENCE

August 2005

Major Subject: Atmospheric Sciences

**RETRIEVAL OF OPTICAL AND MICROPHYSICAL PROPERTIES
OF ICE CLOUDS USING ATMOSPHERIC RADIATION
MEASUREMENT (ARM) DATA**

A Thesis

by

JACQUELINE ANNE KINNEY

Submitted to the Office of Graduate Studies of
Texas A&M University
in partial fulfillment of the requirements for the degree of
MASTER OF SCIENCE

Approved by:

Chair of Committee,
Committee Members,

Head of Department,

Ping Yang
Thomas Wilheit
Gerald North
George Kattawar
Richard Orville

August 2005

Major Subject: Atmospheric Sciences

ABSTRACT

Retrieval of Optical and Microphysical Properties of Ice Clouds Using Atmospheric Radiation Measurement (ARM) Data. (August 2005)

Jacqueline Anne Kinney, B.S., Texas A&M University

Chair of Advisory Committee: Dr. Ping Yang

The research presented here retrieves the cloud optical thickness and particle effective size of cirrus clouds using surface radiation measurements obtained during the Atmospheric Radiation Measurement (ARM) field campaign. The algorithm used is based on a method proposed by Yang *et al.* (2005). The research examines single-layer ice clouds in the midlatitude and polar regions. The retrieved information in the midlatitudes is then verified using retrievals from the Moderate-resolution Imaging Spectroradiometer (MODIS) onboard the Terra and Aqua satellites.

DEDICATION

This thesis is dedicated to my friends and family who have always helped and supported me throughout my life.

ACKNOWLEDGEMENTS

I would like to thank Dr. Ping Yang, my advisor, for his guidance and support. I would like to thank him for giving me the opportunity to continue my education, and for the encouragement to continue further. I would also like to thank Heli Wei who offered much support throughout this project. Without him, this study would never have been completed. I would like to thank the members of my committee, Dr. Thomas Wilheit, Dr. Gerald North, and Dr. George Kattawar, for supporting my research and for giving their time to assist in editing this thesis.

This study was supported by the National Science Foundation, under grant ATM-458131, and the NASA Radiation Sciences Program under grant NAG5-12120.

Data were obtained from the Atmospheric Radiation Measurement (ARM) Program sponsored by the U.S. Department of Energy, Office of Science, Office of Biological and Environmental Research, Climate Change Research Division.

Finally, I would like to thank my family and friends for all their support throughout the years. I especially would like to thank Danny Lynch, my fiancé, for all his love, support, and encouragement.

TABLE OF CONTENTS

	Page
ABSTRACT.....	iii
DEDICATION.....	iv
ACKNOWLEDGEMENTS.....	v
TABLE OF CONTENTS.....	vi
LIST OF FIGURES.....	vii
LIST OF TABLES.....	x
1. INTRODUCTION.....	1
2. SCATTERING AND RADIATIVE TRANSFER MODELS.....	5
a. Single-scattering Properties of Ice Crystals.....	5
b. Single-scattering Properties of Ice Clouds.....	8
c. Line-by-line Model.....	11
d. DISORT Model.....	14
e. Fast Cloud Model.....	15
3. METHODOLOGY.....	19
a. Case Selection.....	19
b. Gamma Technique.....	20
c. Retrieval Algorithm.....	23
4. DATA.....	28
5. RESULTS.....	33
a. Southern Great Plains (SGP).....	33
b. North Slope of Alaska (NSA).....	49
6. CONCLUSIONS.....	58
REFERENCES.....	60
VITA.....	63

LIST OF FIGURES

FIGURE	Page
1	Comparison of the computed phase function for hexagonal columns and the Henyey-Greenstein phase function for two effective particle sizes..... 6
2	Schematic of IR radiation received at the surface..... 17
3	Measured and calculated clear-sky radiance profiles before (top) and after (middle) the gamma fitting technique was applied..... 22
4	Downward radiance and corresponding enveloping profile used in this study to calculate the slope/average value pair..... 24
5	Radiance profile for two effective sizes computed using the fast model..... 25
6	Radiance profile for various optical thicknesses computed using the fast model..... 26
7	Example lookup table that relates the slope of region I and the average value of region II to effective size and optical thickness..... 27
8	Sky image taken at 1715 UTC on August 18, 2003 (a) and the cloud-base height as determined by the MPL on the same date (b)..... 30
9	Sky image taken at 1500 UTC on August 14, 2002 (a) and the cloud-base height as determined by the MPL on the same date (b)..... 31
10	MPL-calculated cloud-base height for 02/05/2003..... 35
11	MPL-calculated cloud-base height for 08/17/2003..... 35
12	MPL-calculated cloud-base height for 01/05/2004..... 36
13	MPL-calculated cloud-base height for 02/10/2004..... 36
14	Retrieved optical thickness (top) and effective size (bottom) for 02/05/2003..... 38

FIGURE		Page
15	Retrieved optical thickness (top) and effective size (bottom) for 08/17/2003.....	38
16	Retrieved optical thickness (top) and effective size (bottom) for 01/05/2004.....	39
17	Retrieved optical thickness (top) and effective size (bottom) for 02/10/2004.....	39
18	MPL-calculated cloud base height for 03/08/2003.....	41
19	MPL-calculated cloud base height for 03/31/2003.....	41
20	MPL-calculated cloud base height for 04/07/2003.....	42
21	MPL-calculated cloud base height for 01/28/2004.....	42
22	MPL-calculated cloud base height for 12/15/2004.....	43
23	Retrieved optical thickness (top) and effective size (bottom) for 03/08/ 2003.....	46
24	Retrieved optical thickness (top) and effective size (bottom) for 03/31/2003.....	46
25	Retrieved optical thickness (top) and effective size (bottom) for 04/07/2003.....	47
26	Retrieved optical thickness (top) and effective size (bottom) for 01/28/2004.....	47
27	Retrieved optical thickness (top) and effective size (bottom) for 12/15/2004.....	48
28	MPL-calculated cloud base height for 11/06/2002 at NSA.....	50
29	MPL-calculated cloud base height for 11/07/2002 at NSA.....	51
30	MPL-calculated cloud base height for 11/25/2002 at NSA.....	51
31	MPL-calculated cloud base height for 01/29/2003 at NSA.....	52

FIGURE	Page
32 MPL-calculated cloud base height for 05/07/2003 at NSA.....	52
33 Retrieved optical thickness (top) and effective size (bottom) for 11/06/2002.....	54
34 Retrieved optical thickness (top) and effective size (bottom) for 11/07/2002.....	54
35 Retrieved optical thickness (top) and effective size (bottom) for 11/25/2002.....	55
36 Retrieved optical thickness (top) and effective size (bottom) for 01/29/2003.....	55
37 Retrieved optical thickness (top) and effective size (bottom) for 05/07/2003.....	56

LIST OF TABLES

TABLE		Page
1	Nighttime cases for the SGP.....	34
2	Cloud information for daytime SGP cases.....	40
3	Our retrieved values of optical thickness and effective size and MODIS values of optical thickness and effective size.....	45
4	NSA cloud cases.....	49

1. INTRODUCTION

Cirrus clouds occur regularly throughout the globe and therefore they have a significant impact on the earth's radiation energy budget. To improve the accuracy and reliability of numerical weather prediction and general climate models, clouds and their interactions with the atmospheric radiation budget must be appropriately described (Lynch *et al.*, 2002). This is difficult because cirrus clouds have been identified as one of the least understood components in climate research (Liou, 1986). Cirrus clouds impact the earth's radiation budget because they reflect incoming solar radiation back to space (albedo effect) and trap outgoing terrestrial thermal emission from the lower atmosphere and the surface (greenhouse effect). Which effect dominates is determined by the microphysical and radiative properties of cirrus clouds (Stephens *et al.*, 1990). The degree and extent of this greenhouse vs. albedo effect will lead to atmospheric differential cooling and heating (Liou, 1986).

Over the past decade many research efforts have focused on understanding the radiative and microphysical properties of cirrus clouds, and several methods have been introduced to determine these cloud properties using radiation measurements in the infrared region. For example, Smith *et al.* (1993) derived the longwave radiative properties (i.e., spectral emissivity and reflectivity) of clouds using the 8-12 μm (820-1250 cm^{-1}) spectral window region. This was achieved by carefully selecting the cloud particle size and cloud water content, which minimized the absolute difference of the ratio of the retrieved emissivity to the theoretical emissivity of the cloud. Collard *et al.*

This thesis follows the style of *Journal of Atmospheric Sciences*.

(1995) used Smith's method and expanded it to the 1800-3000 cm^{-1} wavenumber region, which he referred to as the Band II region (note that the region used by Smith *et al.* (1993) is referred to as the Band I region). DeSlover and Smith (1999) used the Atmospheric Emitted Radiance Interferometer (AERI) (Smith *et al.*, 1995) data to investigate the cirrus cloud visible-to-infrared spectral optical depth ratios in 18 infrared microwindows.

Wei *et al.* (2004) developed two methods to retrieve the optical thickness of semitransparent ice clouds. One method used the spectral brightness temperatures at atmospheric window channels (1070-1135 cm^{-1}), and the other used two brightness temperature differences (900-1559 K and 1587-1559 K). They then applied these methods to data acquired from the Atmospheric Infrared Sounder (AIRS) satellite instrument. A fast cloud model was also developed for use in this study.

Huang *et al.* (2004) used the brightness temperature in the atmospheric window region to retrieve the ice cloud microphysical properties. In their study, the cloud particle effective size is determined by matching the slope of a simulated brightness temperature in the 790-960 cm^{-1} spectrum band to the observed spectrum. Optical thickness is then derived by matching the observed and the simulated spectrums in the 1100-1250 cm^{-1} band using the values of effective size determined in the previous step.

Yang *et al.* (2005a) introduced a technique similar to that developed by Huang *et al.* (2004) for retrieving the optical and microphysical properties of cirrus clouds. The former technique uses radiance measurements (instead of brightness temperature) in the terrestrial infrared window. This technique uses a linear fitting of the minimum

radiances at two microwindows: region I (820-960 cm^{-1}), and region II (1100-1240 cm^{-1}). The slope of the linear fitting of region I and the intercept of the linear fitting of region II are compared to a pre-computed look-up table which was made using a Line-by-line and DISORT model. This technique can be applied to ground-based radiance measurements or space-borne measurements. Guo *et al.* (2005) then used this technique to determine the optical and microphysical properties of cirrus clouds using ground-based infrared radiometric measurements retrieved from the Cirrus Layers Florida Area Cirrus Experiment (CRYSTAL-FACE) field campaign in July 2002.

These studies represent only a small cross-section of the studies, which have focused on the remote sensing of ice clouds using radiances at the infrared wavelengths. The atmospheric infrared window (800-1200 cm^{-1}) is used because the atmospheric gases (except ozone) absorb little radiation, and the spectral signature of the surface radiance in this region is sensitive to the microphysical and optical properties of cirrus clouds (Smith *et al.* 1993).

The intent of the present study is to simultaneously retrieve the cloud optical thickness and the particle effective size using IR radiance measured at the earth's surface. The approach is based on the technique introduced by Yang *et al.* (2005a). The ice cloud microphysical properties will be retrieved for locations in the midlatitude and the polar regions using data collected by the U. S. Department of Energy (DOE) Atmospheric Radiation Measurement (ARM) field campaign. The results from this study should help to improve the understanding of cirrus clouds, and can be used to improve

the accuracy and reliability of numerical weather prediction and general circulation models used to study the weather and climate systems.

Furthermore, we will examine the retrieval method introduced by Yang *et al.* (2005a), and will consider the differences in ice cloud properties in the polar and midlatitude regions. The data used in this study was obtained from the U.S. Department of Energy (DOE) Atmospheric Radiation Measurement (ARM) field campaign.

This thesis is organized as follows. Section 2 of this thesis shows the calculation of the single-scattering properties of ice crystals, and will provide an overview of the models used in this study. Section 3 discusses the method for selecting cases, and the retrieval algorithm used. Finally, Sections 4 and 5 presents retrieval results and conclusions.

2. SCATTERING AND RADIATIVE TRANSFER MODELS

a. Single-scattering Properties of Ice Crystals

The extinction efficiency, single-scattering albedo, and phase function of ice crystals are required to exactly specify the bulk radiative effects of clouds. The present study uses the well-known Henyey Greenstein (H-G) phase function to describe the phase function of cloud particles, which is given by the equation

$$P_{HG}(\theta) = \frac{1 - g^2}{(1 + g^2 + 2 \cos \theta)^{3/2}} = \sum_{l=0}^N (2l + 1) g^l P_l(\cos \theta), \quad (1)$$

where θ is the scattering angle and g is the asymmetry factor of cloud particles. The asymmetry factor can be calculated using

$$g = \frac{1}{2} \int_0^\pi P(\theta) \cos(\theta) \sin(\theta) d\theta, \quad (2)$$

where $P(\theta)$ is the phase function. In Eq. (1), $P_l(\cos \theta)$ is the l^{th} Legendre polynomial.

For the H-G phase function, the l^{th} expansion coefficients of the phase function is

simply the l^{th} power of g . Because of this, using the H-G phase function is simple and

efficient for numerical computation. Figure 1 shows that the H-G phase function is close

to the actual phase function derived for hexagonal ice crystals. The technical details for

computing the single-scattering properties of ice crystals for wavelengths ranging from 3

μm to 100 μm have been reported by Yang *et al.* (2005b), who used a combination of

the finite-difference time domain (FDTD) technique (Yee, 1996; Yang and Liou, 1996a),

an improved geometric optics method (Yang and Liou, 1996b), and the Lorenz-Mie

theory, following the composite approach developed by Fu *et al.* (1998).

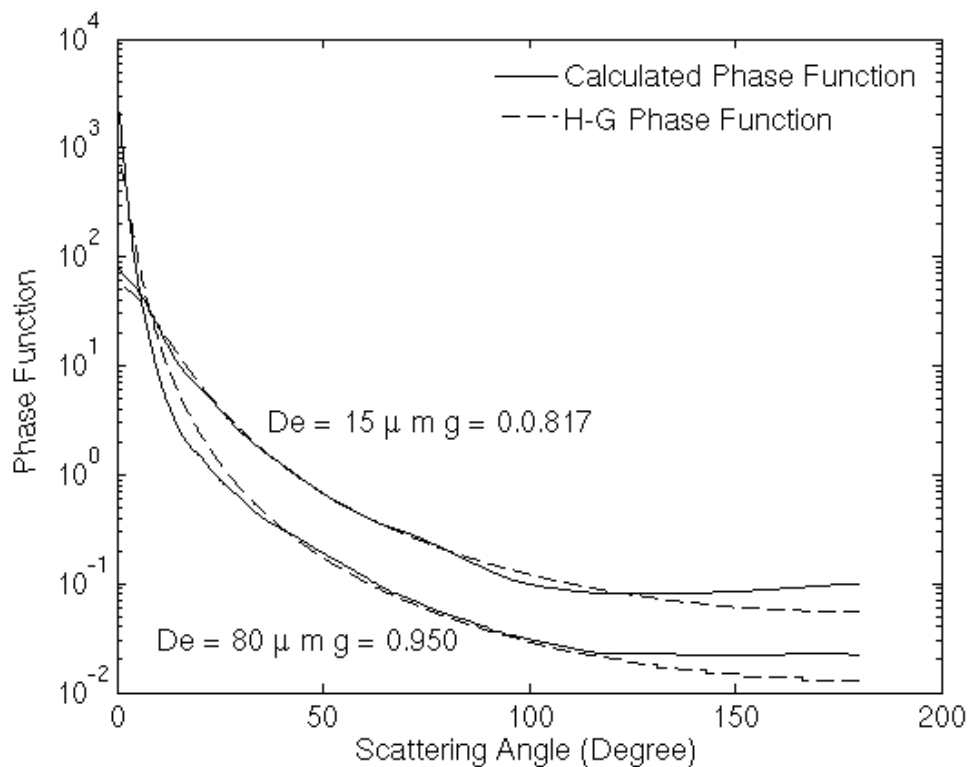


FIG. 1. Comparison of the computed phase function for hexagonal columns and the Henyey-Greenstein phase function for two effective particle sizes.

Cirrus clouds are composed of nonspherical ice particles, and particle size, refractive index, and shape affect the single-scattering properties of ice crystals. In this study, the shapes of cirrus cloud particles are simplified as hexagonal columns, and the single-scattering properties are calculated for 201 wavenumbers between 500 and 2500 cm^{-1} in steps of 10 cm^{-1} . The scattering data not directly calculated can easily be interpolated because the refractive index varies relatively weakly with wavelength.

The aspect ratio for ice crystals as defined by Yang *et al.* (2001) is

$$2a/L = \begin{cases} 1, & L \leq 40 \mu\text{m}, \\ \exp[-0.017835(L - 40)], & 40 < L \leq 50 \mu\text{m}, \\ 5.916/L^{1/2}, & L > 50 \mu\text{m}, \end{cases} \quad (3)$$

where a is the semi-width of a cross-section and L is the length of an ice crystal (maximum dimension of a column). This distribution is used to define the three-dimensional geometry of an ice crystal for the scattering computations, and is in agreement with observations previously reported. (Ono, 1969; Aure and Veal, 1970)

There are various methods available for computing the single-scattering properties of nonspherical ice crystal particles. In this study a combination of three methods were used. For particles with sizes less than 40 μm , the FDTD results are used. For larger particles a composite method was used (Wei *et al.*, 2004; Fu *et al.*, 1998). This composite method is based on the fact that the Lorenz-Mie theory as applied to equivalent spheres has been found to overestimate the scattering and absorption efficiencies for hexagonal columns, and Geometric Optics Method (GOM) has been found to underestimate the absorption efficiencies (Yang *et al.*, 2001). The solution is therefore a weighted summation of the results of GOM applied to hexagonal ice crystals and Lorenz-Mie applied to equivalent spheres. The weighting factors are selected so that there is no discontinuity between the FDTD solution and the composite result.

For the application of the Mie theory, nonspherical particles must first be converted into equivalent spheres. Fu *et al.* (1998) found that Lorenz-Mie theory with equal-ratio of volume to projected area yields better results than the exact FDTD

method. Following Grenfell and Warren (1999) and Fu *et al.* (1998), we define the size of the equivalent sphere for a hexagonal ice crystal as:

$$D_e = \frac{3}{2} \left(\frac{\text{Volume}}{\text{Projected Area}} \right) = \frac{3\sqrt{3}a^2L}{\sqrt{3a^2 + 2aL}}, \quad (4)$$

where a and L have been previously defined.

b. Single-scattering Properties of Ice Clouds

To compute the mean single-scattering properties for cirrus clouds we need to include the size distribution of ice crystals because cirrus clouds are composed of nonspherical ice crystals of all sizes. In this study the 30 size distributions compiled by Fu *et al.* (1998) from various sources in this literature are selected. These distributions were obtained during various field campaigns by measuring a variety of midlatitude and tropical cirrus clouds.

We can define the mean single-scattering properties for cirrus clouds as follows in equations (5) – (8). Mean extinction efficiency of cirrus clouds:

$$\langle Q_e \rangle = \frac{\int_{L_{\min}}^{L_{\max}} Q_e(L)A(L)n(L)dL}{\int_{L_{\min}}^{L_{\max}} A(L)n(L)dL}. \quad (5)$$

Mean absorption efficiency of cirrus clouds:

$$\langle Q_a \rangle = \frac{\int_{L_{\min}}^{L_{\max}} Q_a(L)A(L)n(L)dL}{\int_{L_{\min}}^{L_{\max}} A(L)n(L)dL}. \quad (6)$$

Mean asymmetry factor of cirrus clouds:

$$\langle g \rangle = \frac{\int_{L_{\min}}^{L_{\max}} g(L) [Q_e(L) - Q_a(L)] A(L) n(L) dL}{\int_{L_{\min}}^{L_{\max}} [Q_e(L) - Q_a(L)] A(L) n(L) dL}, \quad (7)$$

and mean single-scattering albedo of cirrus clouds:

$$\langle \omega \rangle = \frac{\int_{L_{\min}}^{L_{\max}} [Q_e(L) - Q_a(L)] A(L) n(L) dL}{\int_{L_{\min}}^{L_{\max}} Q_e(L) A(L) n(L) dL} = \frac{\langle Q_e \rangle - \langle Q_a \rangle}{\langle Q_e \rangle}, \quad (8)$$

where $Q_e(L)$ and $Q_a(L)$ are the extinction and absorption efficiencies calculated for ice crystals with size L . $A(L)$ is the projected area, $n(L)$ is the particle number density, and L_{\min} and L_{\max} are the minimum and maximum sizes in the size distribution.

Following Foot (1988) and Francis *et al.* (1994), we define the effective size of a nonspherical ice crystal on the basis of the ratio of total volume to projected-area.

Specifically, the effective size of cirrus clouds is similarly defined as:

$$D_e = \frac{3 \int_{L_{\min}}^{L_{\max}} V(L) n(L) dL}{2 \int_{L_{\min}}^{L_{\max}} A(L) n(L) dL}, \quad (9)$$

where $V(L)$ is the volume of an ice particle with size L . This effective size is used as a measure of the average size of the cloud particles for a given size distribution.

The mean single-scattering properties are parameterized at each wavelength with respect to the effective size of ice crystals using a third order polynomial function. The parameterizations are given by the following equations:

$$\langle Q_e \rangle = C_{e0} + C_{e1} D_e + C_{e2} D_e^2 + C_{e3} D_e^3, \quad (10)$$

$$\langle Q_a \rangle = C_{a0} + C_{a1} D_e + C_{a2} D_e^2 + C_{a3} D_e^3, \quad (11)$$

$$\langle g \rangle = C_{g0} + C_{g1}D_e + C_{g2}D_e^2 + C_{g3}D_e^3, \quad (12)$$

where C_{ij} ($i = e, a, g; j = 0, 1, 2, 3$) is the fitted coefficient and is a function of wavelength. The fitted coefficients are computed for the same 201 wavenumbers used for calculating the single-scattering properties of ice crystals, and 30 size distributions are used covering an effective size range from 15-154 μm . These coefficients are then stored in a database for easy use.

The radiative properties of real cirrus clouds are related to the optical thickness or ice water content (IWC) of cirrus clouds. The ice water content is given by

$$IWC = \rho_{ice} \int_{L_{min}}^{L_{max}} (L)V(L)n(L)dL, \quad (13)$$

where ρ_{ice} is the mass density of ice. The extinction coefficient is given by:

$$\beta = \int_{L_{min}}^{L_{max}} Q_e(L)A(L)n(L)dL. \quad (14)$$

Combining equations (5),(9), and (13) with equation (14) we get:

$$\beta = \frac{3}{2} \frac{IWC}{D_e \rho_{ice}} \langle Q_e \rangle. \quad (15)$$

The optical thickness is:

$$\tau = \beta \Delta z = \frac{3}{2} \frac{IWC}{D_e \rho_{ice}} \langle Q_e \rangle \Delta z, \quad (16)$$

where Δz is the physical thickness of the cloud.

The path of integration of ice content in cirrus clouds is known as the ice water path (IWP) and is simply the IWC multiplied by the physical thickness of the cloud.

Using this, we can then rewrite equation (16) in terms of IWP as follows:

$$\tau = \frac{3}{2} \frac{IWP}{D_e \rho_{ice}} \langle Q_e \rangle. \quad (17)$$

The radiative properties of cirrus clouds can be described using IWP by using equation (14) or in terms of the visible optical thickness τ_{vis} . The optical thickness can be calculated from the visible optical thickness using the equation:

$$\tau = \frac{\langle Q_e \rangle}{2} \tau_{vis}. \quad (18)$$

Given IWP or the visible optical thickness and the effective size of the cirrus clouds, we can calculate optical thickness, single-scattering albedo, and asymmetry factor. The scattering phase function can be derived from the asymmetry factor by assuming the Henyey-Greenstein function. Using these properties, we can then simulate the radiative effects of cirrus clouds in the IR region.

c. Line-by-line Model

For this study, we use a line-by-line (LBL) model (Heidinger, 1998) combined with the well-known discrete ordinates radiative transfer (DISORT) model (Stamnes *et al.*, 1988). The LBL model is used to compute the cloud-free atmospheric optical thickness profile. To do this the atmosphere is assumed to be plane-parallel, and it is divided into a discrete number of layers. Each layer is homogeneous and has a temperature T_j , pressure p_j , and thickness Δz_j where j denotes the j^{th} atmospheric layer. In this study 100 layers are used, and the sounding profile provides the atmospheric pressure, temperature, and relative humidity for each layer. For each layer

we first calculate the absorption coefficient, $k_{v,j,n}$, for each gas. This is done using the equation:

$$k_{v,j,n} = \sum_{l=1}^L k_{v,j,n,l} = \sum_{l=1}^L S_{n,l}(T_j) f_{v,n,l}(T_j, P_j), \quad (19)$$

where n denotes the n^{th} gas, $l = 1 \dots L$ and is the number of absorbing lines at a selected wavenumber ν . $f_{v,n,l}$ and $S_{v,n,l}$ are the absorption line shape and the line intensity, respectively, of the l^{th} absorbing line. For very high pressure we can use the Lorentz shape, for very low-pressure we use the Doppler shape, and a Voigt line shape is used for the pressures in between. The Lorentz line shape is the shape caused by collisions of air molecules and is given by the equation

$$f = \frac{\alpha_L}{\pi(\nu - \nu_0)^2 + \alpha_L^2}, \quad (20)$$

where ν_0 is the wavenumber of an ideal, monochromatic line, and α is the half-width of the line at the half-maximum. The Doppler shape is used for very low pressures when there are very few collisions between molecules. The Doppler line shape is given by

$$f_D = \frac{1}{\alpha_D \sqrt{\pi}} \exp\left[-\left(\frac{\nu - \nu_0}{\alpha_D}\right)^2\right], \quad (21)$$

where $\alpha_D = \nu_0 \left(2KT/mc^2\right)^{1/2}$ is a measure of the Doppler width of the line (K is the Boltzmann constant, T is the absolute temperature, m is the mass of the molecule, and c is the velocity of light). Finally, the Voigt profile is a convolution of the Lorentz and Doppler line shapes. The Doppler line redistributes the Lorentz line at wavenumber ν'

to ν . The line shapes may then be expressed by $f(\nu' - \nu_0)$ and $f_D(\nu - \nu')$. The convolution of these two profiles is given by

$$f_V = \frac{1}{\alpha_D \sqrt{\pi}} K(x, y), \quad (22)$$

where the Voigt function is defined by

$$K(x, y) = \frac{y}{\pi} \int_{-\infty}^{\infty} \frac{1}{y^2 + (x-t)^2} e^{-t^2} dt. \quad (23)$$

For simplicity, we have let $t = (\nu - \nu') / \alpha_D$, $y = \alpha / \alpha_D$, and $x = (\nu - \nu_0) / \alpha_D$ (Liou, 2002).

Once the absorption coefficient is calculated the optical depth of each gas can be calculated using:

$$\tau_{v,j,n} = k_{v,n,j} u_{n,j}, \quad (24)$$

where $u_{n,j}$ is the amount of the n^{th} gas in that layer. Finally, to calculate the total optical depth for each layer, we sum the optical depth of each gas in the layer.

$$\tau_{v,j} = \sum_{n=1}^N \tau_{v,j,n}, \quad (25)$$

This process is then repeated for each atmospheric layer.

For the for the LBL model used in this study, the spectral line parameters are provided by the HITRAN-2000 data set (Rothman, *et al.*, 2003). Except for line absorption, the continuum absorption by water vapor and other gases are considered.

d. DISORT Model

The DISORT equations are based on the theory of Chandrasekhar (1960). The code used in this study is available to the public and was originally developed by Stamnes *et al.* (1988).

DISORT calculates the transfer of monochromatic radiation at frequency $\tilde{\nu}$ through a plane-parallel medium using the equation

$$\mu \frac{du_{\tilde{\nu}}(\tau_{\tilde{\nu}}, \mu, \phi)}{d\tau} = u_{\tilde{\nu}}(\tau_{\tilde{\nu}}, \mu, \phi) - S_{\tilde{\nu}}(\tau_{\tilde{\nu}}, \mu, \phi), \quad (26)$$

where $u_{\tilde{\nu}}(\tau_{\tilde{\nu}}, \mu, \phi)$ is the specific intensity in the direction (μ, ϕ) at optical depth $\tau_{\tilde{\nu}}$, which is measured perpendicular to the surface of the medium. The azimuthal angle of the medium is ϕ , and μ is the cosine of the polar angle. The source function $S_{\tilde{\nu}}$ is given by

$$S_{\tilde{\nu}}(\tau_{\tilde{\nu}}, \mu, \phi) = \frac{\omega_{\tilde{\nu}}(\tau_{\tilde{\nu}})}{4\pi} \int_0^{2\pi} d\phi' \int_{-1}^1 d\mu' P_{\tilde{\nu}}(\tau_{\tilde{\nu}}, \mu, \phi; \mu', \phi') \times u_{\tilde{\nu}}(\tau_{\tilde{\nu}}, \mu', \phi') + Q_{\tilde{\nu}}(\tau_{\tilde{\nu}}, \mu, \phi), \quad (27)$$

where $\omega_{\tilde{\nu}}(\tau_{\tilde{\nu}})$ is the single-scattering albedo, and $P_{\tilde{\nu}}(\tau_{\tilde{\nu}}, \mu, \phi; \mu', \phi')$ is the phase function. The source term ($Q_{\tilde{\nu}}(\tau_{\tilde{\nu}}, \mu, \phi)$) is described by equations (28) – (30).

$$Q_{\tilde{\nu}}(\tau_{\tilde{\nu}}, \mu, \phi) = Q_{\tilde{\nu}}^{(thermal)}(\tau_{\tilde{\nu}}) + Q_{\tilde{\nu}}^{(beam)}(\tau_{\tilde{\nu}}, \mu, \phi) \quad (28)$$

$$Q_{\tilde{\nu}}^{(thermal)}(\tau_{\tilde{\nu}}) = [1 - \omega_{\tilde{\nu}}(\tau_{\tilde{\nu}})] B_{\tilde{\nu}}[T(\tau_{\tilde{\nu}})] \quad (29)$$

$$Q_{\tilde{\nu}}^{(beam)}(\tau_{\tilde{\nu}}, \mu, \phi) = \frac{\omega_{\tilde{\nu}}(\tau_{\tilde{\nu}}) I_0}{4\pi} P_{\tilde{\nu}}(\tau_{\tilde{\nu}}, \mu, \phi; \mu_0, \phi_0) \exp\left(-\frac{\tau_{\tilde{\nu}}}{\mu_0}\right) \quad (30)$$

Equation (29) is the source term for thermal emission in local thermodynamic equilibrium. Equation (30) is the source term for parallel beam incident radiation in the direction (μ_0, ϕ_0) on a nonemitting medium, and $I_0\mu_0$ is the incident flux.

In the model, it is assumed that the medium consists of L adjacent homogeneous layers (100 in the case of this study). The single-scattering albedo and phase function are assumed to be constant in each layer, but can vary from layer to layer. Our optical thickness, τ , has been calculated for each layer from the LBL model.

A cloud is simulated by adding an optical thickness, single-scattering albedo, and scattering phase function for a single model atmospheric layer.

e. Fast Cloud Model

The combination of the LBL and DISORT models requires significant computational resources; therefore, a fast model has been developed for use in this study. This model is based on the Atmospheric Infrared Sounder (AIRS) clear-sky model (Strow *et al.*, 2003) and a corresponding fast model for radiative transfer in a cloudy atmosphere (Wei *et al.*, 2004). This AIRS models were originally designed to calculate the upwelling radiance at the top of the atmosphere. The model used in this study is a combination of both models, and has been adjusted to calculate the downward radiance received at the surface. In this model, it has been assumed that the clouds are located in a plane-parallel, single homogeneous, and isothermal layer. As shown in Fig. 2, the fast model assumes that the radiance received at the surface is composed of four parts:

1. The atmospheric radiation from the top of the atmosphere that is transmitted

through the cloud layer to the surface, $I_0 \frac{T_{a2}}{T_{a1}} T_{cld}$. Where the atmospheric

radiation, $I_0 = \int_{T_{a1}}^1 B(t) dT_a$, and T_{a1} and T_{a2} are the atmospheric

transmittance from the top of the atmosphere to the cloud and to the surface,

respectively. T_{cld} is the transmittance of the cloud.

2. The radiation emitted from the cloud that is transmitted to the surface

$I_{cld} \frac{T_{a2}}{T_{a1}}$. The radiation emitted from the cloud, I_{cld} , is given by

$I_{cld} = \varepsilon B(t_{cld})$. Where ε is the emissivity of the cloud, and $B(t_{cld})$ is the

Planck's radiance at the cloud temperature.

3. The radiation emitted from the atmosphere layer below the cloud

$\int_{T_{a2}}^{T_{a1}} B(t) dT_a$, where t is the temperature at some layer.

4. The radiation emitted by the surface that is reflected by the cloud

$I_1^\uparrow \frac{T_{a2}}{T_{a1}} R_{cld}(\mu)$. Where the upward radiation received by the cloud base is

given by $I_1^\uparrow = \varepsilon B(t_s) \frac{T_{a2}}{T_{a1}} + \int_{T_{a2}}^{T_{a1}} B(t) dT_a$. Where t_s is the temperature at the

surface.

The total radiation received at the surface is assumed to be the sum of these four parts

$$I_{sur}(\mu) = \left[\int_{T_{a1}}^1 B(t) dT_a \right] \frac{T_{a2}}{T_{a1}} T_{cld} + \varepsilon B(t_{cld}) \frac{T_{a2}}{T_{a1}} + \int_{T_{a2}}^{T_{a1}} B(t) dT_a + \left[\varepsilon B(t_s) \frac{T_{a2}}{T_{a1}} + \int_{T_{a2}}^{T_{a1}} B(t) dT_a \right] \frac{T_{a2}}{T_{a1}} R_{cld}(\mu) \quad (31)$$

T_a is calculated from the AIRS clear-sky model. If the albedo and transmissivity of the cloud are known, the radiance at the surface, $I_{sur}(\mu)$, in Eq. (31) would be easy to calculate.

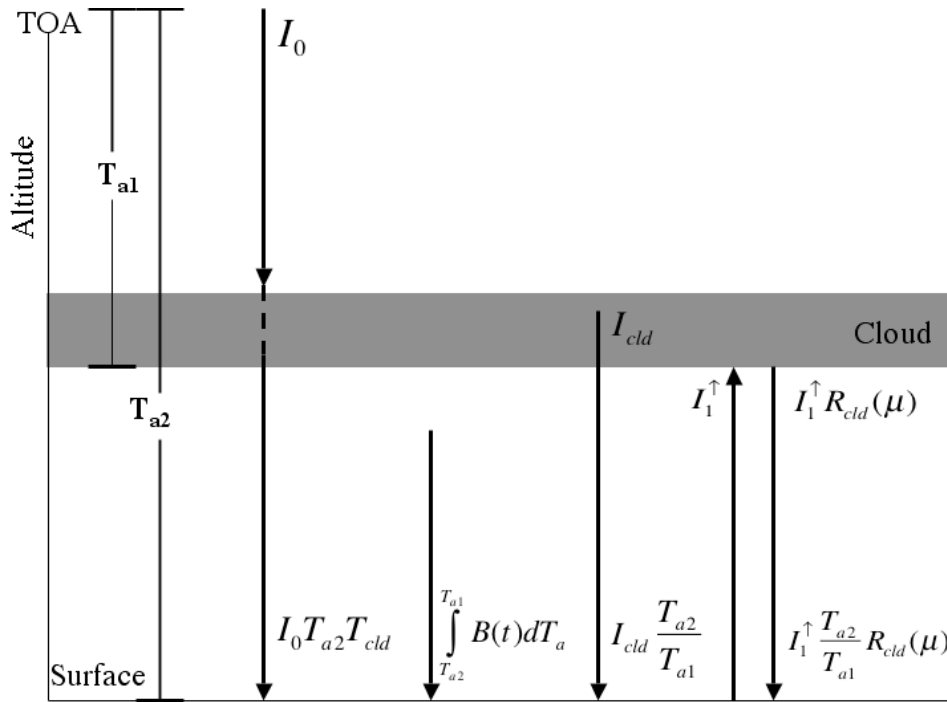


FIG. 2. Schematic of IR radiation received at the surface.

The albedo and transmissivity function for cirrus clouds are calculated 50 optical thicknesses (0.4-100) and 50 effective sizes (10-157 μm) at 201 wavenumbers using the DISORT model. This database is too large to efficiently use, so we express the transmissivity and albedo as a third order polynomial which is a function of effective size for a certain wavenumber and optical thickness. The fitted coefficients are then determined for the 201 wavenumbers and 50 optical thicknesses, and a database of the fitted coefficients for the transmissivity function is created as well as a database of the fitted coefficients for the albedo function. Using these databases, we can rapidly obtain the transmissivity and albedo function for cirrus clouds for a specific optical thickness, effective size, and wavenumber.

To simulate a cloudy radiance at the surface, we simply specify an effective size, optical thickness of the cloud, and temperature for a given model layer. We can get the albedo and transmissivity from the pre-calculated fitted coefficient database and then calculate the radiance at the surface using the equations previously discussed.

3. METHODOLOGY

In this study it is assumed that clouds are single-layer, homogenous ice clouds. Therefore, cases must be chosen carefully. Once a case is selected the fast model is run for a clear-sky case and the calculated radiance is matched to the measured radiance. This is done by adjusting the calculated transmittance profile using a technique introduced by Smith *et al.* (1993) known as the “gamma technique”. Once this is completed, the transmittance profile is used to calculate the downward radiance for cloudy cases with various optical thicknesses and effective sizes. Finally, from this model data a lookup table is created from which the optical thickness and effective size can be simultaneously retrieved.

a. Case Selection

For this study cases were selected based on several criteria. First, because it is assumed in the model, the clouds being examined must be single-layer ice clouds. It is also necessary for the gamma adjustment that for each time period examined that there is an adjacent clear-sky time period. There must also be a sounding profile available that is close in time to the time period being examined. Finally, for (Moderate-resolution Imaging Spectroradiometer (MODIS) validation to be completed, the case must take place during the day.

b. Gamma Technique

The cloud-free surface radiance provides the background transmittance profile of the atmosphere and is used in the computation of surface radiance under cloudy conditions. As shown by Collard *et al.*(1995), this profile is critical to the retrieval of optical thickness and effective size. In order to reduce the error in our retrievals, we first match the clear-sky calculated radiance to the clear-sky measured radiance. This is achieved by using a method developed by Smith *et al.* (1993) referred to as the “gamma technique” . For our measured clear-sky radiance profile, we select a radiance profile as close in time as possible to the cloudy time period that is being examined. To match these measured and calculated clear-sky radiances adjustments are made to the transmittance profile that was calculated by the fast model using the following equation:

$$T^*(\nu) = T_0(\nu)^{\gamma(\nu)}, \quad (32)$$

where T is the transmittance profile and is a function of wavenumber and atmospheric layer.

The gamma term is a function of wavelength and is calculated using the following iterative formula:

$$\gamma_n(\nu) = \gamma_{n-1}(\nu) + \frac{\gamma_{n-1}(\nu) - \gamma_{n-2}(\nu)}{R_c(\gamma_{n-1}) - R_c(\gamma_{n-2})} [R_m(\nu) - R_c(\gamma_{n-1})], \quad (33)$$

where $R_m(\nu)$ is the measured clear-sky radiance and $R_c(\gamma_{n-1})$ is the calculated radiance using the transmittance profile that was adjusted using γ_{n-1} . In this study, this iteration is executed twice. Executing the iteration twice gave the best match to the measured radiance.

Sample results for the gamma fit are shown in Fig. 3. The top panel shows the measured and calculated radiance profiles prior to the gamma adjustment, and the middle is the measured and calculated radiance after the gamma adjustment. Looking at these two figures it can be seen that the calculated radiance is a much better match to the measured radiance after the gamma adjustment has been applied. The bottom panel of Fig. 3 shows the percent error between the measured clear-sky radiance and the calculated radiance after the gamma fit was applied. The blue line is 10% error and the red line is 5%. From this it can be easily seen that the error remains under 10% for the wavenumber range used in this study, and the error is under 5% for the majority of the wavenumbers. These figures illustrate that this technique is quite successful in matching the calculated clear-sky radiance to the measured clear-sky radiance.

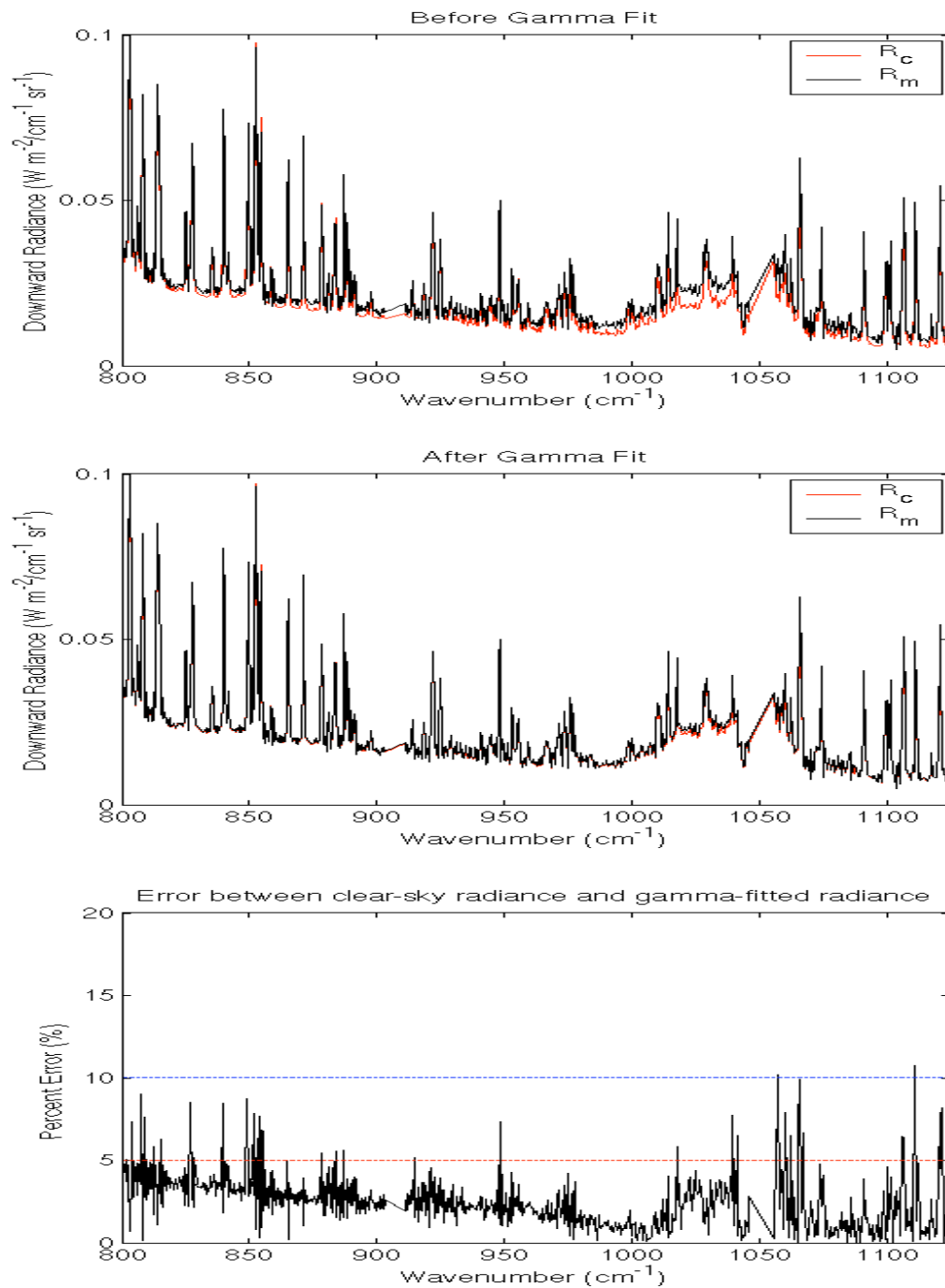


FIG. 3. Measured and calculated clear-sky radiance profiles before (top) and after (middle) the gamma fitting technique was applied. The bottom panel shows the percent error between the actual results and the calculated results after the gamma fitting was applied.

c. Retrieval Algorithm

The retrieval algorithm used in this study relies on a slope/average value pair for each radiance profile. These are determined using the enveloping profiles as shown in Fig. 4. These enveloping profiles are the linear-fitting of the minimum radiance values within two window regions. Region I is the wavenumbers between 820-960 cm^{-1} , and region II is the wavenumbers between 1100-1240 cm^{-1} . For the slope/average value pair we use the slope of the enveloping profile of region I and the average value of the enveloping profile of region II.

Figure 5 shows various radiance profiles that were created using the fast model. The top two panels show two profiles generated using a constant optical thickness of 2.0, and an effective size of 10 μm and 50 μm . The bottom two panels were generated using a constant effective size of 30 μm and an optical thickness of 0.2, 1.0, 2.0, and 5.0. By examining the various radiance profiles shown in Figs. 5 and 6, we can see that the slope of the region I and the average value of region II are sensitive to the effective size and the optical thickness. Because of this sensitivity, each slope/average value pair should have a unique effective size/optical thickness pair. If this is true, we can create a lookup table of cloud optical thickness and particle effective size as shown in Fig. 6. This lookup table is created by running the fast model for 25 optical thicknesses (0.2 - 5 in steps of 0.2) and 25 effective sizes (10 - 106 μm in steps of 4 μm). By comparing the slope/average value pair determined from the measured radiance to the lookup table we can determine the optical thickness and effective size of the cloud. Because of the sensitivity of the radiance to the clear-sky radiance and the cloud height, a new lookup

table is created for each cloud case we examine. By looking at Fig. 7 it can be seen that as the effective size gets large, the ability to accurately retrieve the value decreases.

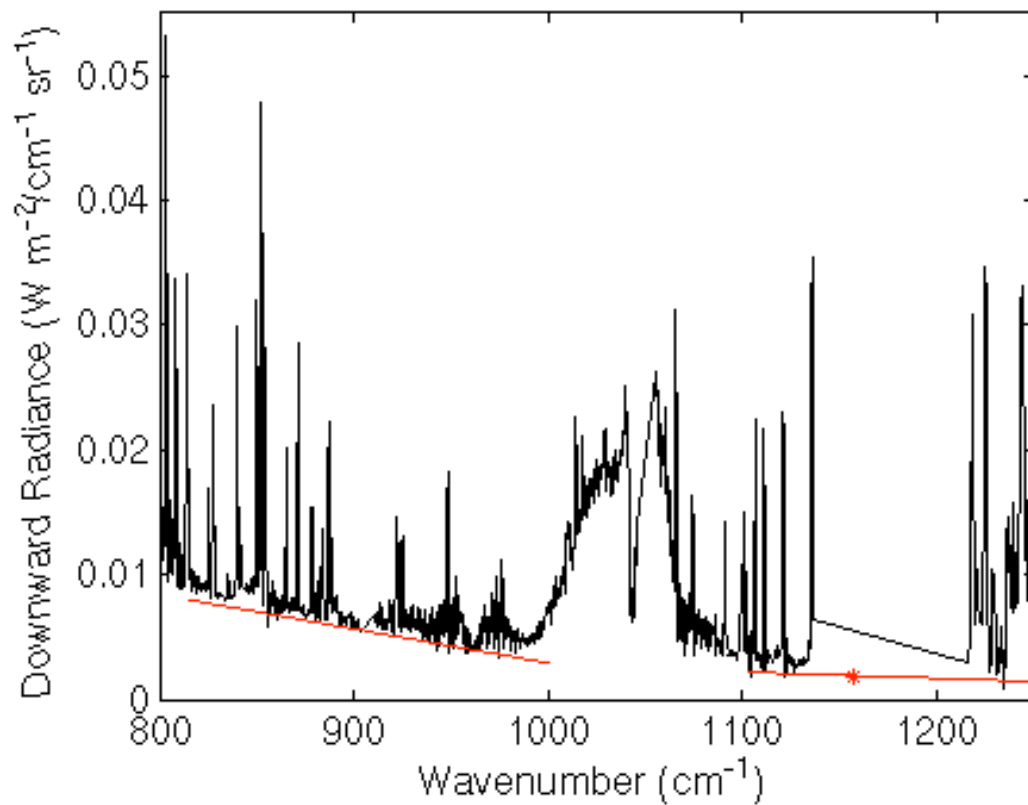


FIG. 4. Downward radiance and corresponding enveloping profile used in this study to calculate the slope/average value pair.

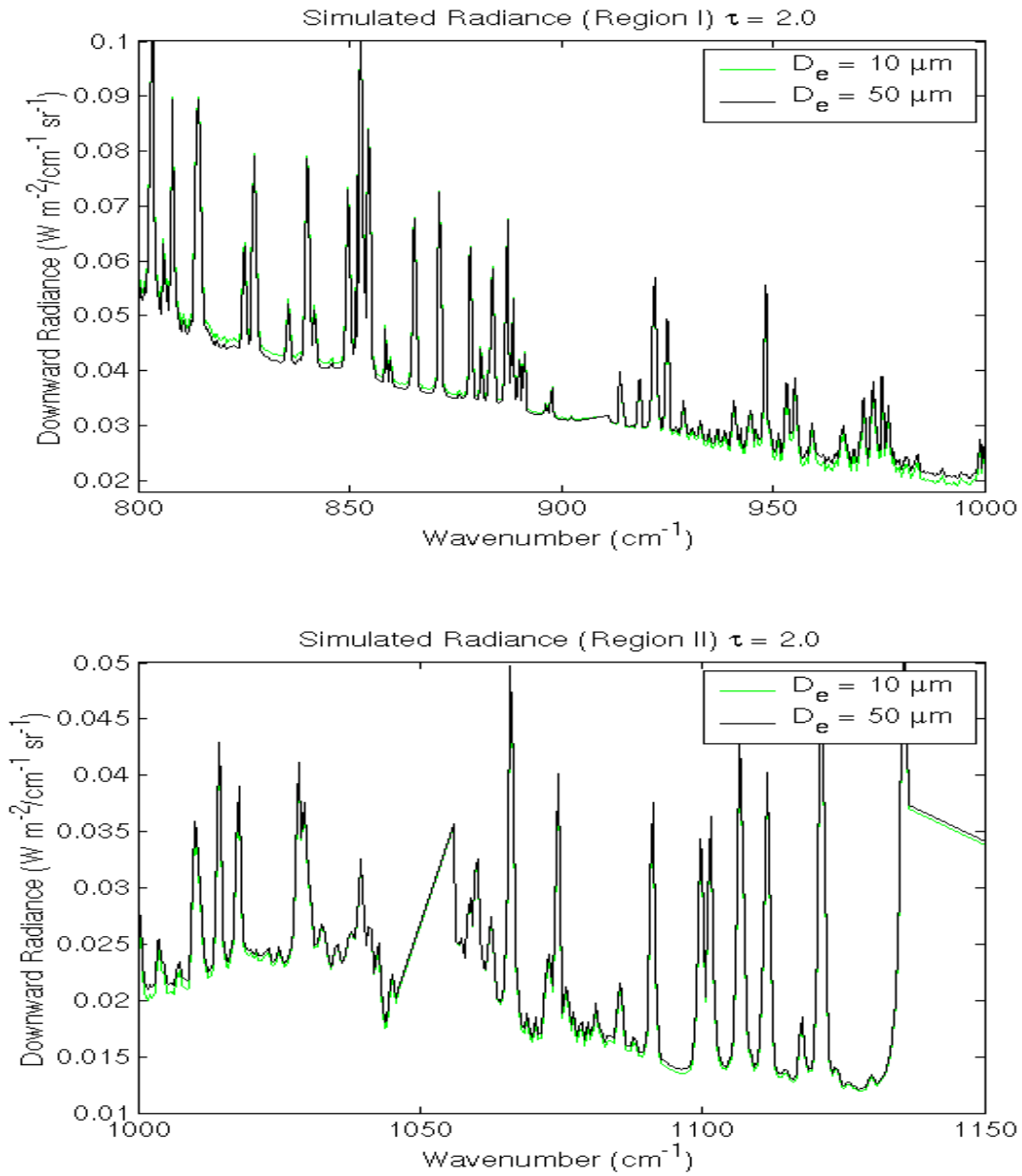


FIG. 5. Radiance profile for two effective sizes computed using the fast model. Optical thickness is held constant at 2.0.

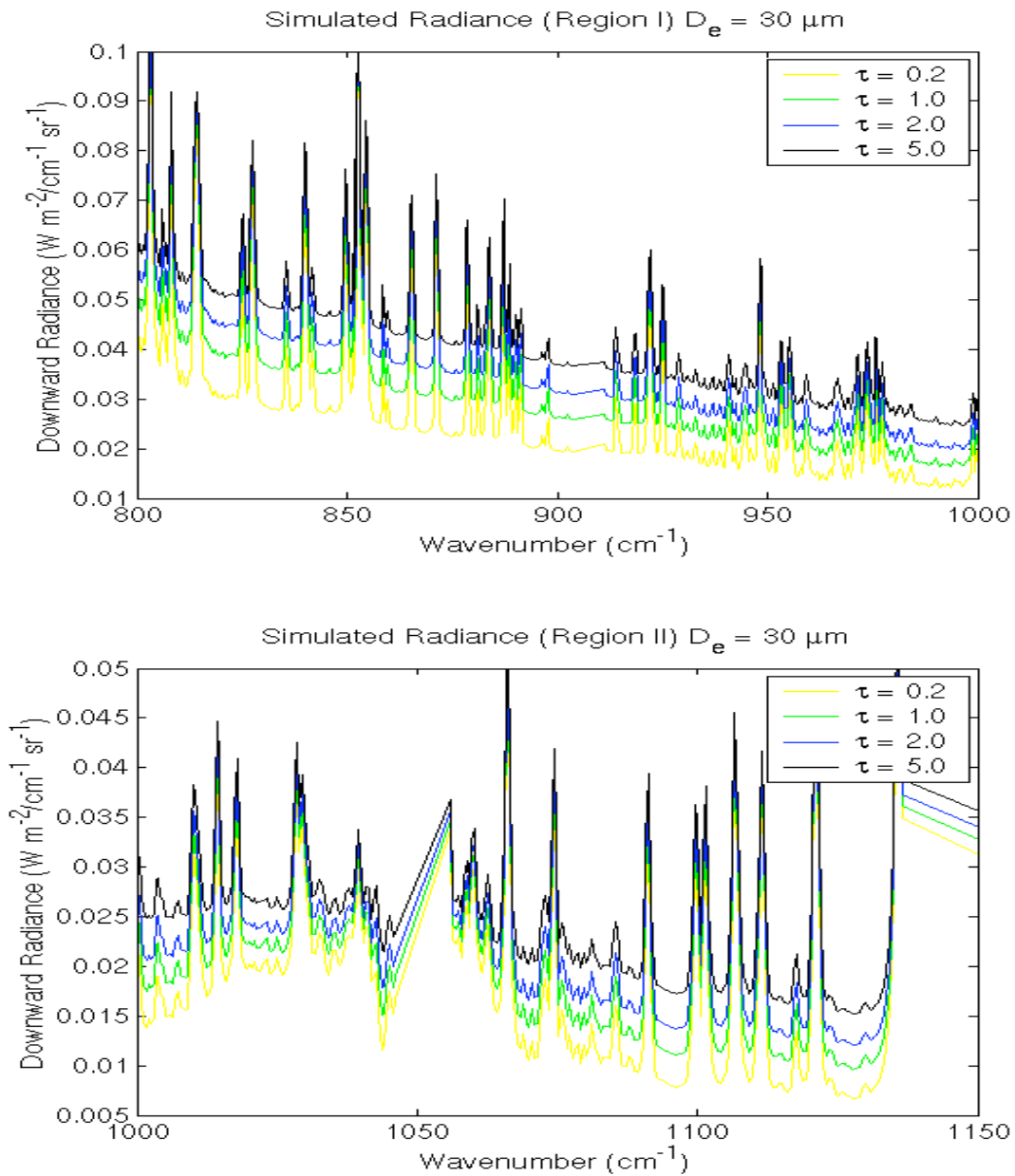


FIG. 6. Radiance profile for various optical thicknesses computed using the fast model. Effective size is held constant at $30\ \mu\text{m}$.

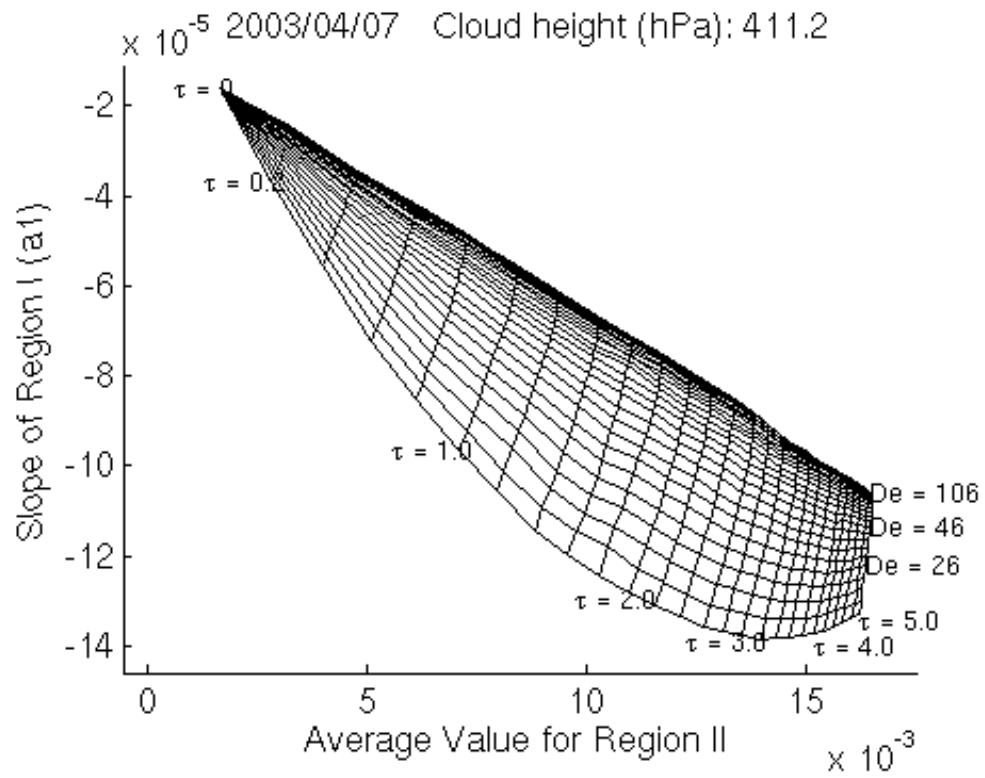


FIG. 7. Example lookup table that relates the slope of region I and the average value of region II to effective size and optical thickness.

4. DATA

Retrievals for this study were made for two locations corresponding to two ARM sites: the Southern Great Plains (SGP) and the North Slope of Alaska (NSA). The SGP site is located in north central Oklahoma at 36° N 97° W 30', and will represent the midlatitudes. SGP was the first ARM measurement site and has data starting in 1993. The NSA site is located at Barrow, Alaska at 71° N 156° W 36.934'. The NSA Barrow facility has data from 1997. The NSA site will represent the polar region.

Three sets of measurements will be used for this study. The measurements are made by similar instruments at each location. Surface radiation measurements are completed by an Atmospheric Emitted Radiance Interferometer (AERI), cloud base height measurements are made by a micropulse lidar (MPL), and atmospheric temperature, pressure, and relative humidity are from a balloon borne sounding system (BBSS).

The AERI instrument measures the absolute infrared spectral radiance ($W / m^2 / sr / cm^{-1}$) of the sky directly above the instrument. The instrument has a spectral range of 500-3300 cm^{-1} at a resolution of 1 cm^{-1} . A calibrated radiance spectrum is produced every 8 minutes. For this study the AERI data is interpolated to match the wavenumber values of the fast model. This allows us to more accurately compare the two profiles.

The MPL is a ground-based optical remote sensing system which is used to determine the altitude of the lowest cloud base directly over the instrument. The MPL operates similar to a radar in that pulses of energy are transmitted into the atmosphere

and some of that energy is scattered back. The cloud-base height is determined using the time delay between the outgoing transmitted pulses and the backscattered signals. The MPL transmits a low-power laser beam and is therefore subject to signal to noise limitations in conjunction with solar background noise. It is also attenuated as it passes through the atmosphere. These two effects make it more difficult to detect high, thin clouds during the day. This had a large impact on this study because it limited our ability to accurately locate high clouds during the day. An example of this effect is shown in Fig. 8. This figure shows the total sky image and the MPL cloud-base height from August 18, 2003. It can be seen in the total sky image from 1715 UTC (Fig 8a.) that there is a cloud overhead, however when you look at Fig 8b which was generated using the MPL-calculated cloud-base heights, it is difficult to tell the cloud-base altitude, and if there are multiple cloud decks. Fig 9 shows a case from August 14, 2002. The sky image is from 1500 UTC. There is no visible cloud in the sky image, however, at the coordinating time period the MPL recorded a scattered signal indicating the possibility of a cloud.

a)



b)

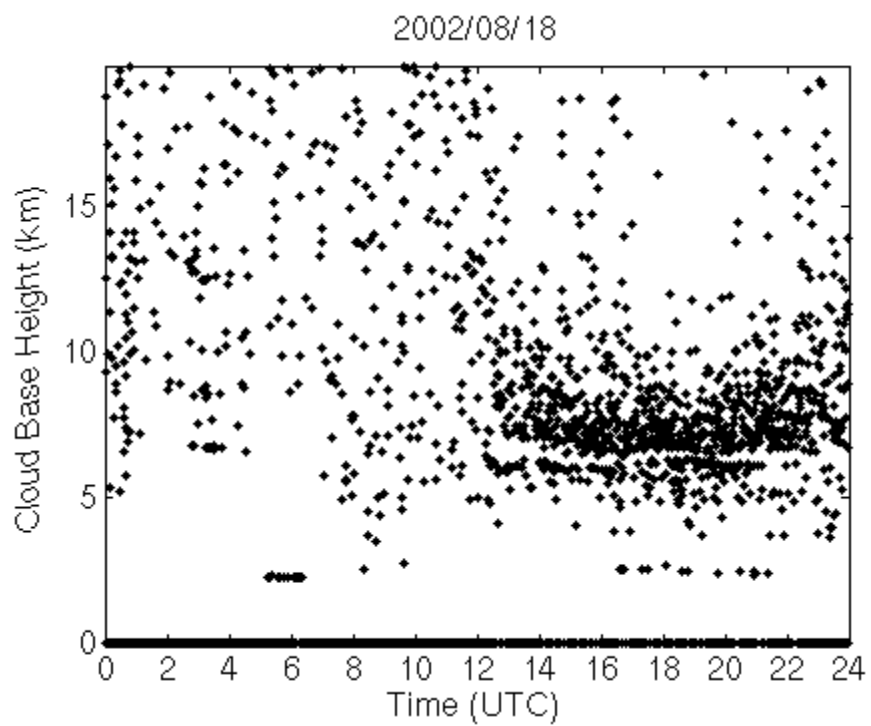


FIG. 8. Sky image taken at 1715 UTC on August 18, 2003 (a) and the cloud-base height as determined by the MPL on the same date (b).

a)



b)

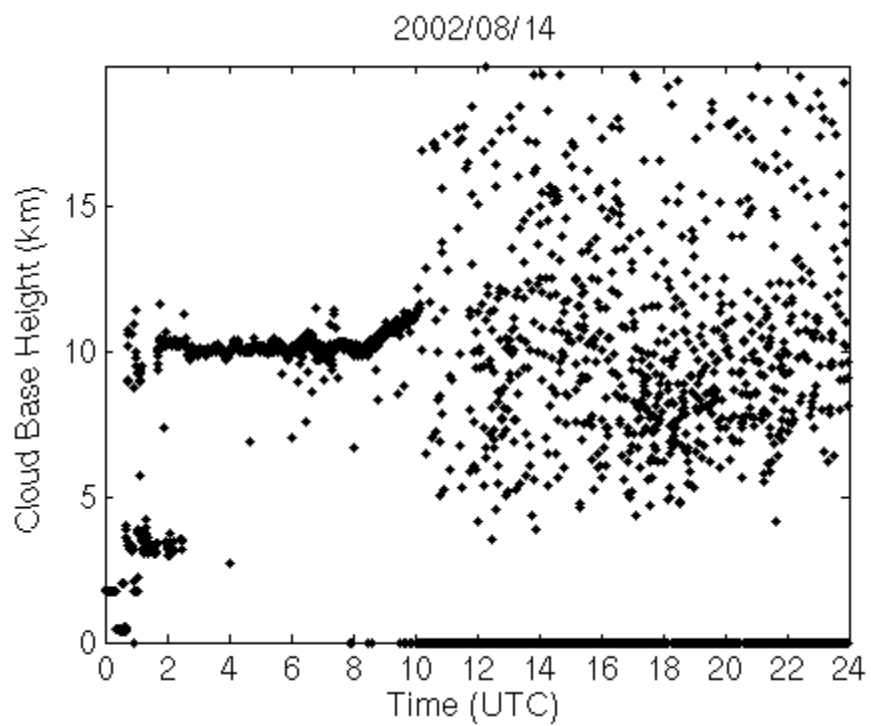


FIG. 9. Sky image taken at 1500 UTC on August 14, 2002 (a) and the cloud-base height as determined by the MPL on the same date (b).

The sounding measurements are taken by a balloon borne sounding system and provide a vertical profile of the atmosphere measuring pressure (hPa), temperature ($^{\circ}\text{C}$), and relative humidity (%). At the SGP site, the balloons are launched 4 times per day and at the NSA site they are launched only once per day. These sounding measurements are used in this study to initialize the LBL model and the fast model.

The validation is completed using the MODIS. The MODIS instrument was developed for the NASA Earth Observing System (EOS) Terra and Aqua satellites which were launched in December 1999 and May 2002, respectively (King, *et al.*, 2003). The Terra and Aqua satellites are polar-orbiting, sun-synchronous, and MODIS provides global coverage every two days (Platnick *et al.*, 2003). Cloud microphysical and optical property retrievals from MODIS are completed at 1 km resolution. The cloud optical thickness and effective size are derived using visible and infrared bands. Because of the use of the visible band, the cloud product is only available during the day (King *et al.*, 2003).

5. RESULTS

As discussed in the retrieval methods section, several cases were carefully selected for each of the two ARM sites, between the years 2002 and 2004. Each site presented unique challenges for the retrievals, and these will be discussed in their respective results section. First we will discuss cases from the SGP and then the NSA.

a. Southern Great Plains (SGP)

This site has the most data available, and therefore, it is the region that was focused on in this study. Nine cases have been divided into night and day in order to investigate some differences found between these two time periods. Also note that, as discussed in the previous section, MODIS validation is only available to be completed on cases occurring during the day.

Four cases were selected for the nighttime, and the cloud information is listed in Table 1. The cloud base heights range from 6.89 to 8.75 km and the cloud base temperatures range from 229.35 to 239.25 K. The warmest cloud base temperature is 239.35 K, therefore it is a reasonable assumption that these clouds are composed mostly of ice crystals.

TABLE 1: Nighttime cases for the SGP.

Date	Time Period (UTC)	Cloud Base Height (km) (hPa)	Cloud Base Temperature (K)
02/05/2003	0300 – 0815	8.75 (317.8)	229.35
08/17/2003	0400 – 0800	7.95 (384.2)	233.55
01/05/2004	0430 – 0720	7.88 (363.8)	239.35
02/10/2004	0425 – 0600	6.89 (416.9)	238.45

Figures 10 -13 show the MPL-measured cloud base height for each case and Figs. 14 -17 show the retrieved optical thickness and effective size for each case. In looking at the MPL figures we can see that the cloud base heights for the night cases are well defined. This made it simple to accurately estimate the cloud-base height. The cloud base heights used in this study are an average over the time period being examined. Looking at the January 5, 2004 case (Fig. 12), we see that the cloud base height is changing over the time period. In cases where this happens, this is a potential source of errors in the retrieval method.

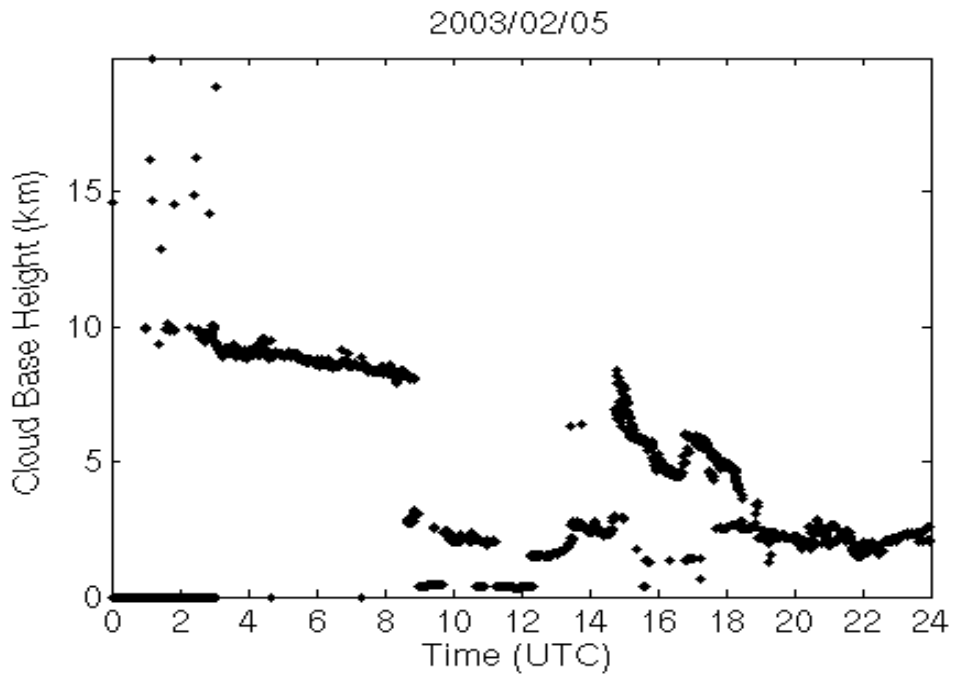


FIG.10. MPL-calculated cloud base height for 02/05/2003.

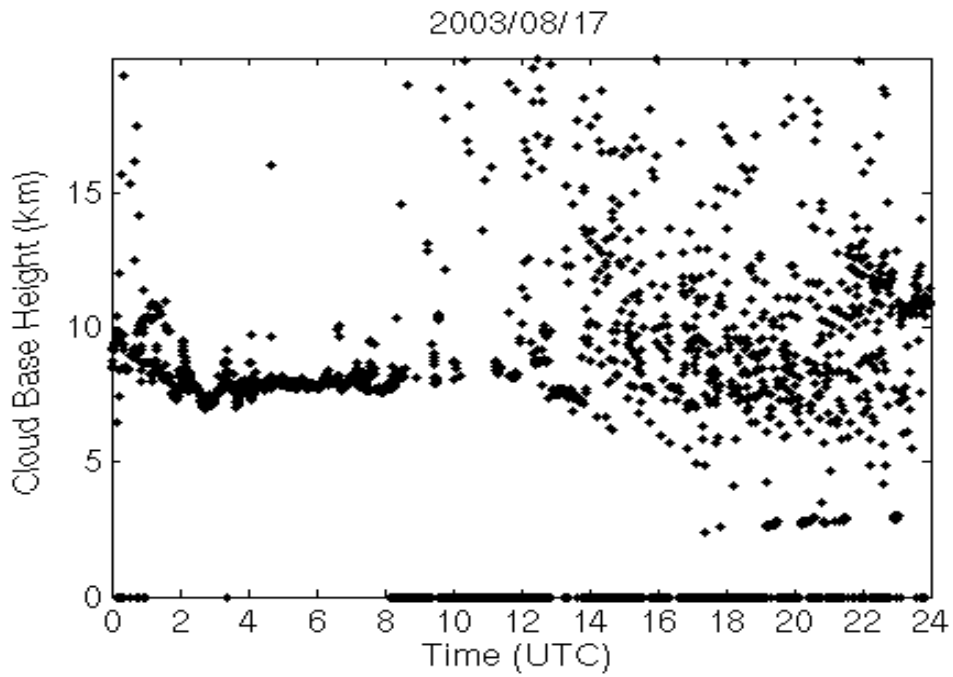


FIG. 11. MPL-calculated cloud base height for 08/17/2003.

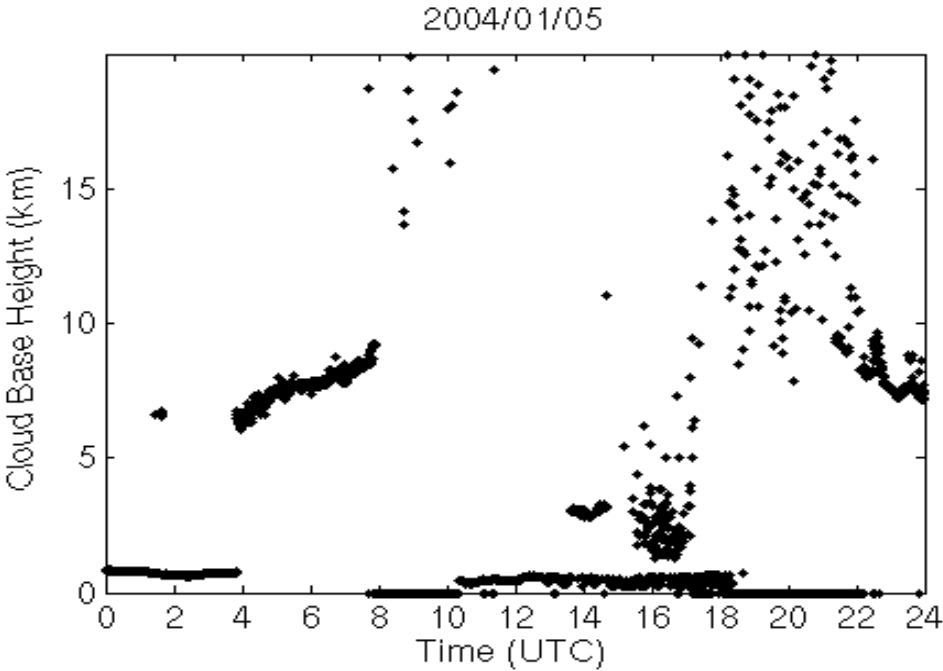


FIG. 12. MPL-calculated cloud base height for 01/05/2004.

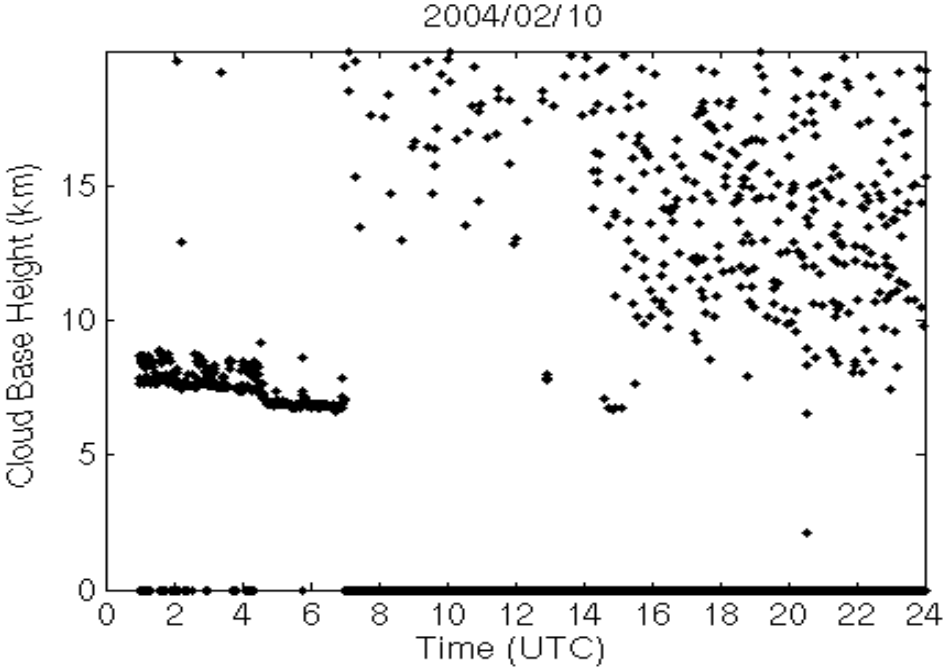


FIG. 13. MPL-calculated cloud base height for 02/10/2004.

We can now examine the retrieved optical thickness and effective size for each case (Figs 14 – 17). Looking at these values we can see a lot of skipping around. It is likely that the cause of some of this jumping is due to different regions of the cloud being measured, or perhaps some lower-level cloud contamination.

On Feb. 5, 2003 the optical thickness ranged from 0.1 to 0.8 with an average of 0.40, and the effective size ranged from 30 to 66 μm with an average of 43.9 μm . On August 17, 2003 the optical thickness ranged from 0.1 to 1.9 with an average of 0.67 and the effective size ranged from 10 to 64 μm with an average of 39.2 μm . It can be seen that there is a general increase then decrease in both the effective size and optical thickness. On January 5, 2004 the optical thickness ranged from 0.1 to 2.1 with an average of 0.6591 and the effective size ranged from 42 to 70 μm with an average of 52.64 μm . There is a sharp increase in optical thickness around 0515 UTC, but the effective size is reasonably constant over the whole time period. February 10, 2004 showed the smallest overall variation with the optical thickness ranging from 0.1 to 0.5 with an average of 0.33 and the effective size ranges from 30 to 54 with an average of 41.

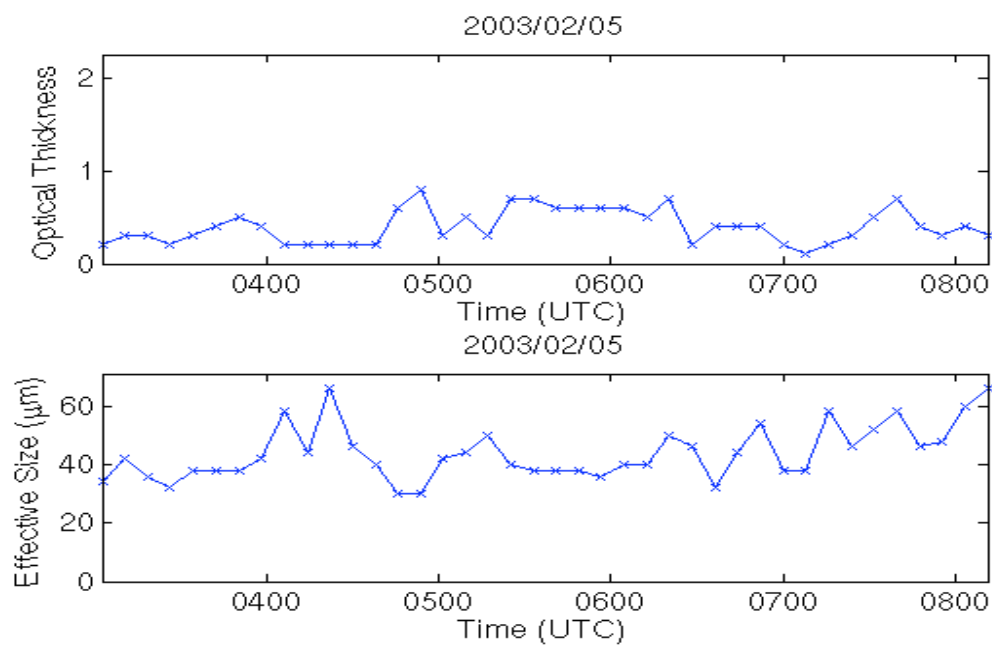


FIG. 14. Retrieved optical thickness (top) and effective size (bottom) for 02/05/2003.

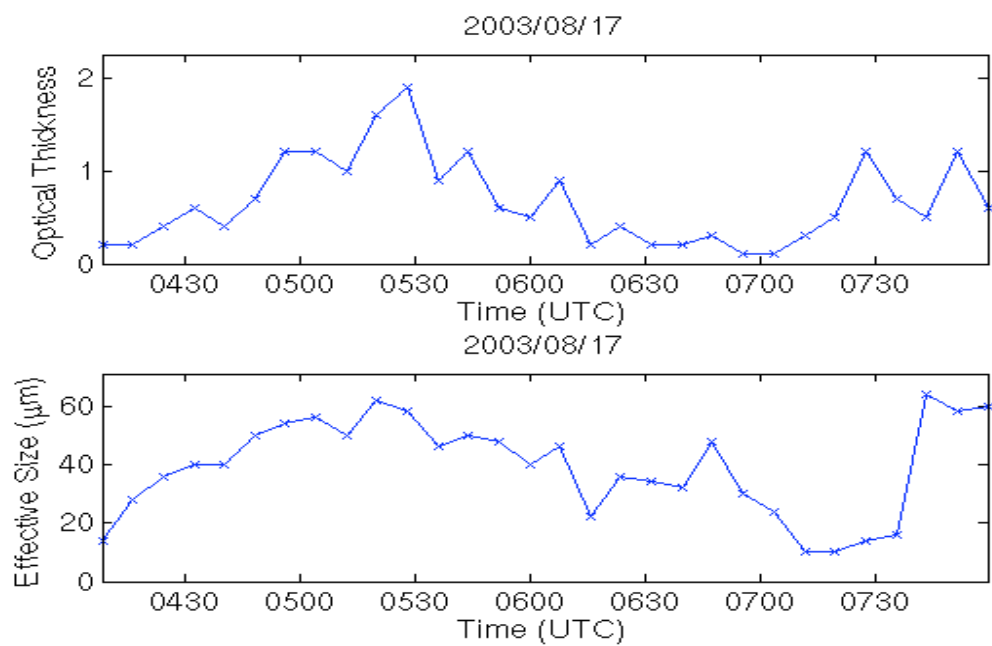


FIG. 15. Retrieved optical thickness (top) and effective size (bottom) for 08/17/2003.

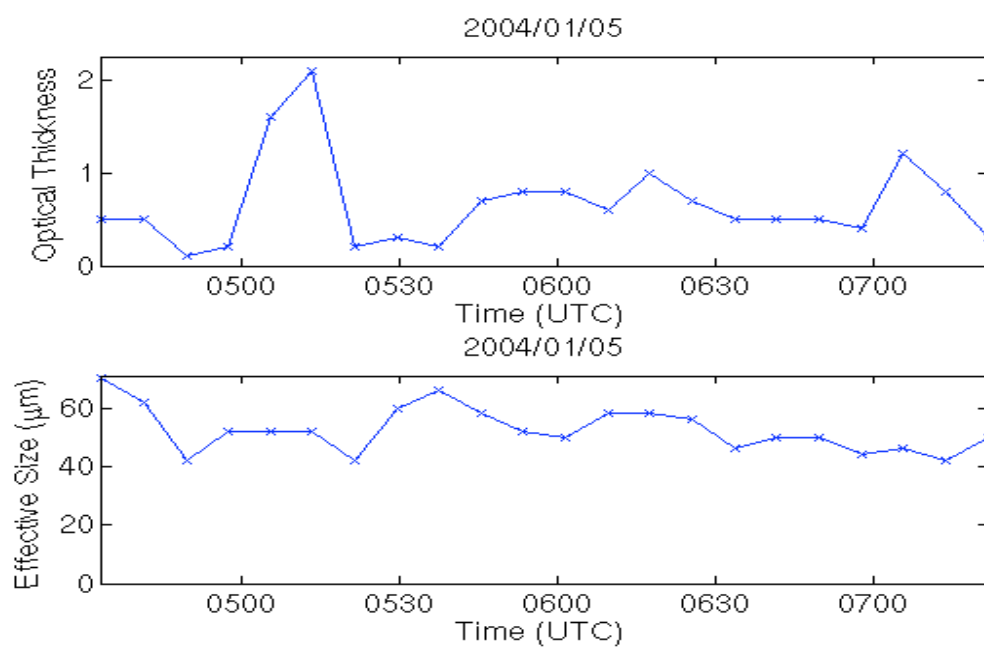


FIG. 16. Retrieved optical thickness (top) and effective size (bottom) for 01/05/2004.

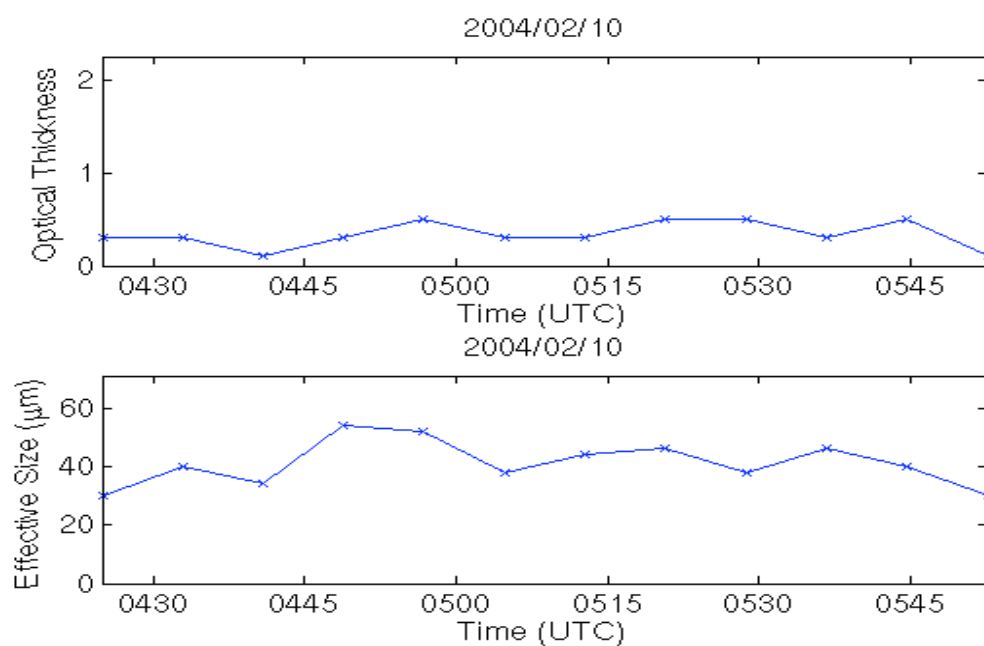


FIG. 17. Retrieved optical thickness (top) and effective size (bottom) for 02/10/2004.

Five cases were selected for the daytime at the SGP location and their cloud information can be found in Table 2. In these cases the cloud base heights ranged from 6.97 to 11.93 and the cloud base temperatures ranged from 223.55K to 244.35K. Again it is assumed that these clouds are composed mostly of ice crystals.

TABLE 2. Cloud information for daytime SGP cases.

Date	Time Period (UTC)	Cloud Base Height (km) (hPa)	Cloud Base Temperature (K)
03/08/2003	1610 – 1830	6.97 (417.3)	244.350
03/31/2003	1315 – 1600	11.07 (238.6)	223.550
04/07/2003	1620 – 1830	7.0 (411.2)	240.550
01/28/2004	1350 – 1745	11.93 (371.8)	232.250
12/15/2004	1445 – 2140	8.0 (361.8)	234.350

Figures 18 - 22 are the MPL cloud base heights and Figs. 23 - 27 are the retrieved optical thickness and effective size for each case. Figures 23, 26, and 27 also have the MODIS retrieved optical thickness and effective size (denoted by an *). There was some difficulty in accurately estimating the cloud base height during the daytime cases because of the MPL errors that were discussed in the data section. By looking at the MPL figures we can see that the cloud base heights are not as clearly defined as they were during the night cases. Therefore in determining the cloud base height for the time period, it was assumed that any scattering outside of the likely location of the cloud are erroneous.

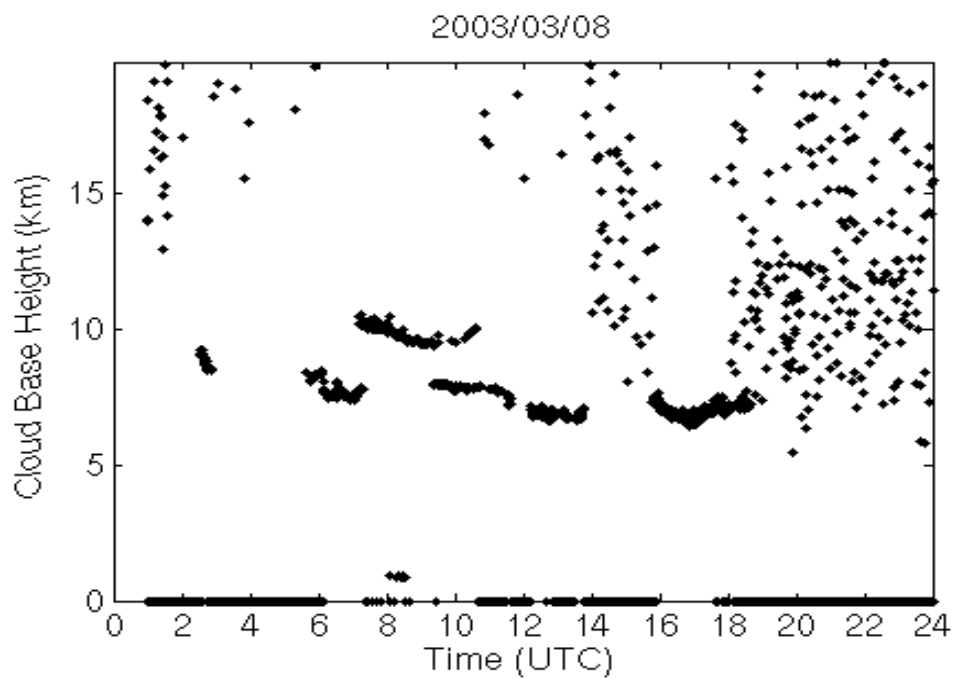


FIG. 18. MPL-calculated cloud base height for 03/08/2003.

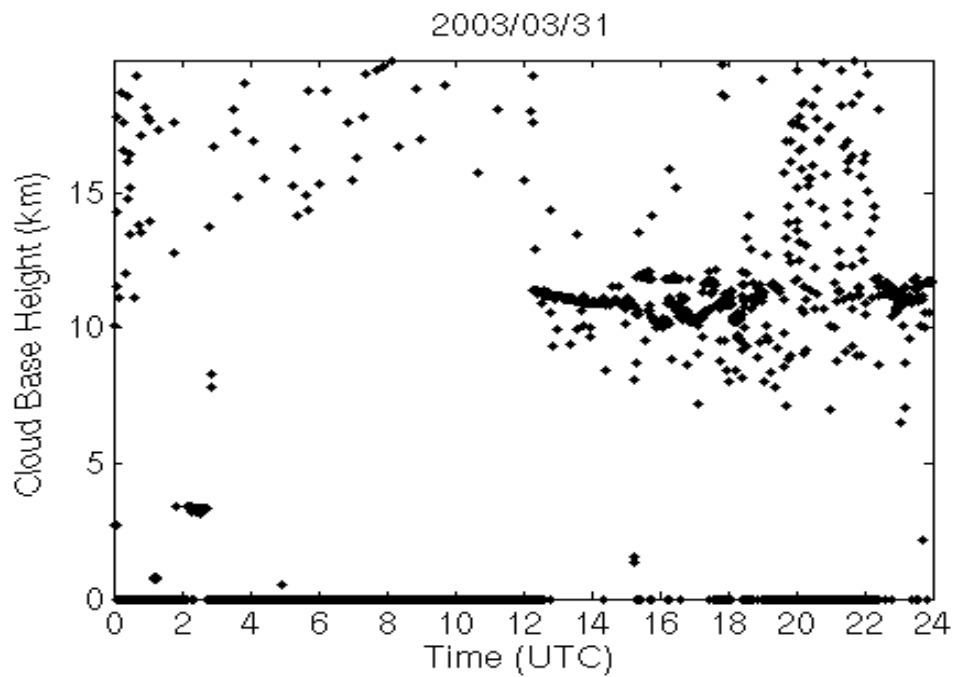


FIG. 19. MPL-calculated cloud base height for 03/31/2003.

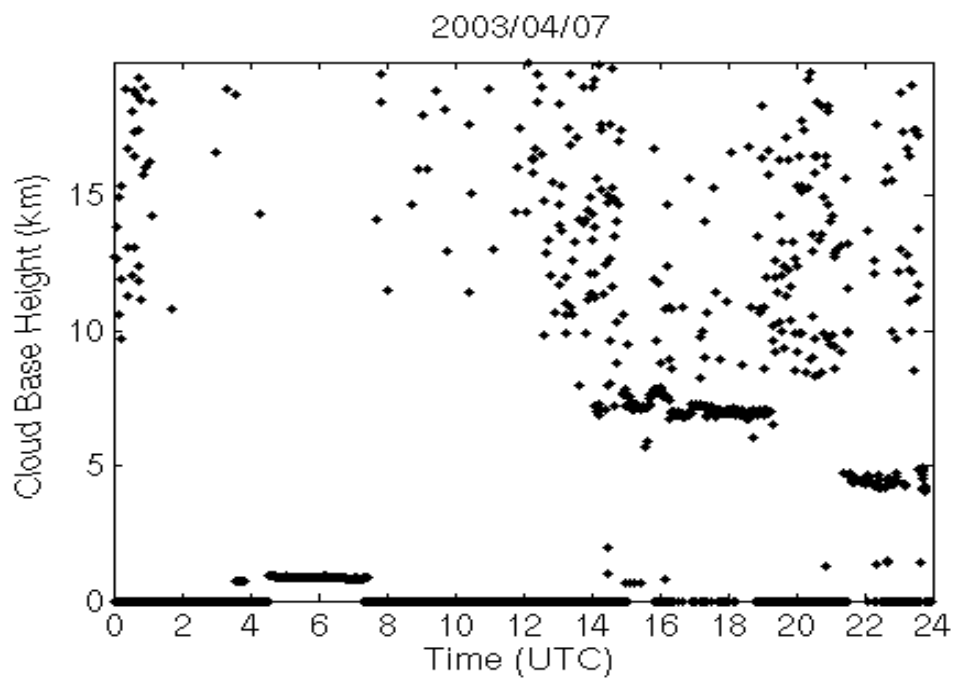


FIG. 20. MPL-calculated cloud base height for 04/07/2003.

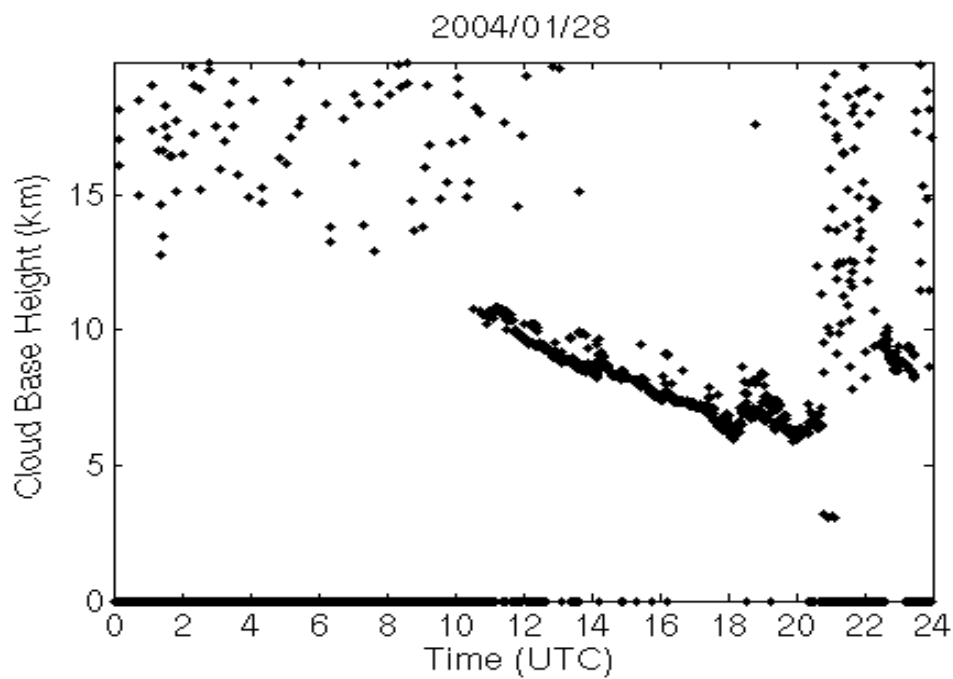


FIG. 21. MPL-calculated cloud base height for 01/28/2004.

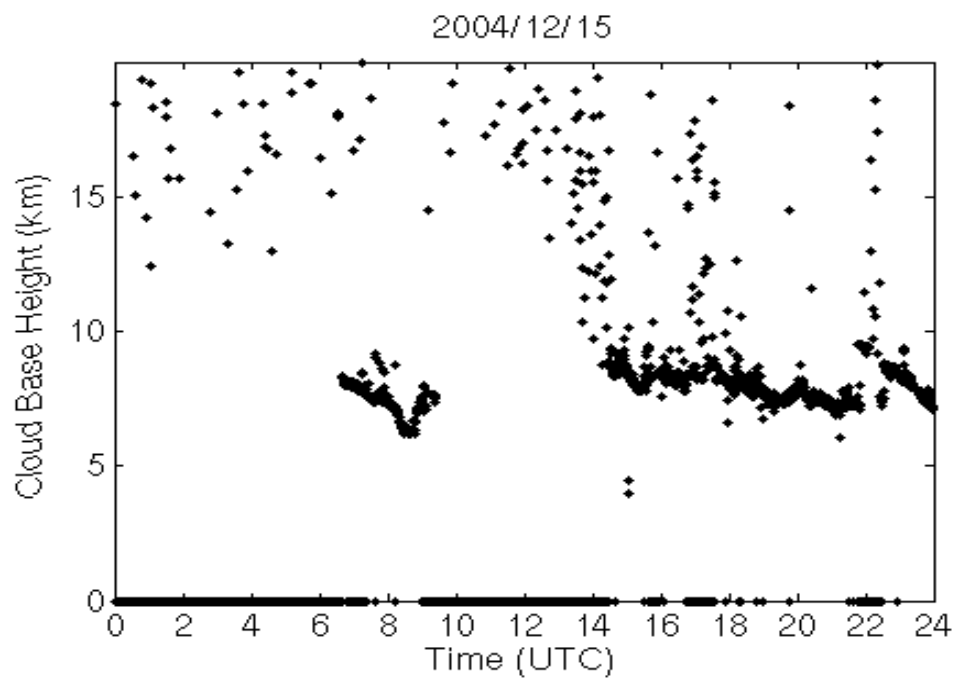


FIG. 22. MPL-calculated cloud base height for 12/15/2004.

Now let's examine the retrieved optical thickness and effective size (Figs. 23-26). On March 8, 2003 the retrieved optical thickness ranged between 0.1 and 0.9 averaging at 0.2533, and the effective size ranged all the way from 10 to 106 μm with an average of 46.8 μm . The optical thickness was constant for most of the time period and there was a large jump in effective size around 1700 UTC. On March 31, 2003 the optical thickness didn't vary much ranging from 0.1 to 0.4 with an average of 0.2571 and the effective size ranged from 10 to 62 μm with an average of 27.05 μm . On April 4, 2003, the optical thickness stayed constant at 0.1 and the effective size ranged from 10 to 44 μm with an average of 24.47 μm . January 28, 2004 the optical thickness ranged from 0.1 to 0.8 with an average of 0.2833 and the effective size ranged from 18 to 70 with an average of 45. Finally, on December 15, 2004, the optical thickness ranged from 0.1 to 1.6 with an average of 0.38 and the effective size ranged from 10 to 54 μm with an average of 34.69 μm .

There seems to be less variability in the optical thickness of the day cases than the night cases. The day cases also have smaller optical thicknesses than the night cases. The night case means ranged from 0.33 to 0.67 while the day means ranged from 0.1 to 0.38. More investigation needs to be completed to conclude if this is a bias in the retrieval method or simply a difference in the cloud properties between night and day.

TABLE 3. Our retrieved values of optical thickness and effective size and MODIS values of optical thickness and effective size.

Date	Time (UTC)	Retrieved Optical thickness	MODIS Optical thickness	Retrieved Effective size (μm)	MODIS Effective size (μm)
2003/03/08	1745	0.1	1.0	16.5	49.8
2004/01/28	1710	0.67	3.0	52	49.9
2004/12/15	1835	0.3	1.0	30	27.6

Table 3 shows the optical thickness and effective sizes retrieved in this study and by MODIS. Comparing the effective size values retrieved in this study with the values retrieved by MODIS we see that our retrieved values are generally quite good. Our effective size significantly underestimated the MODIS effective size on March 8, 2003, but for the other two cases, our values were almost right on. Our retrieved optical thickness is always significantly smaller than the MODIS optical thickness, however. This difference in optical thickness could be due to the bias discussed in the previous paragraph.

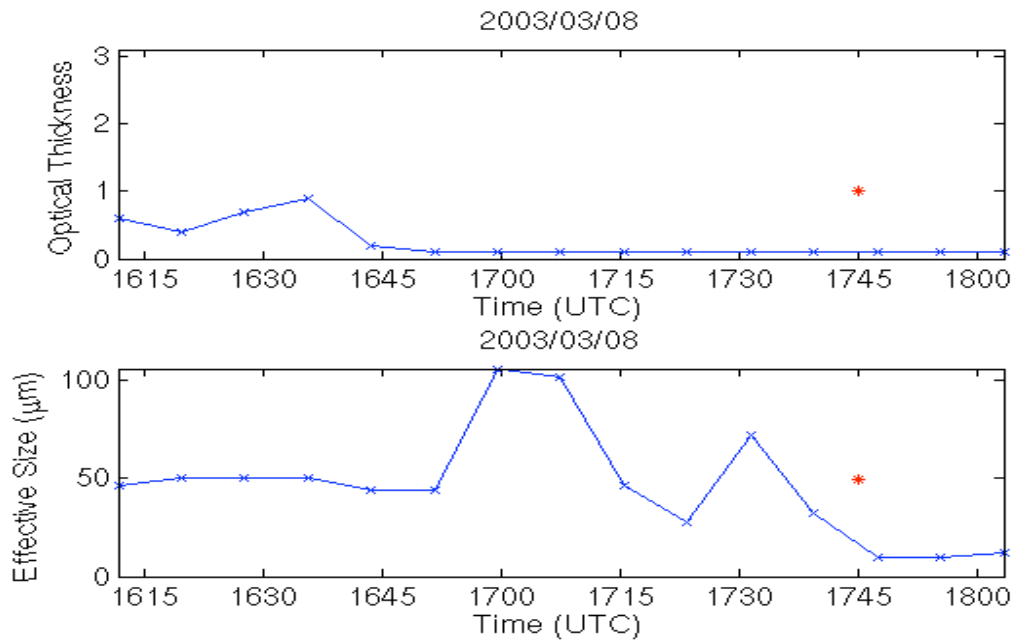


FIG. 23. Retrieved optical thickness (top) and effective size (bottom) for 03/08/2003. MODIS optical thickness and effective size retrievals are denoted by (*).

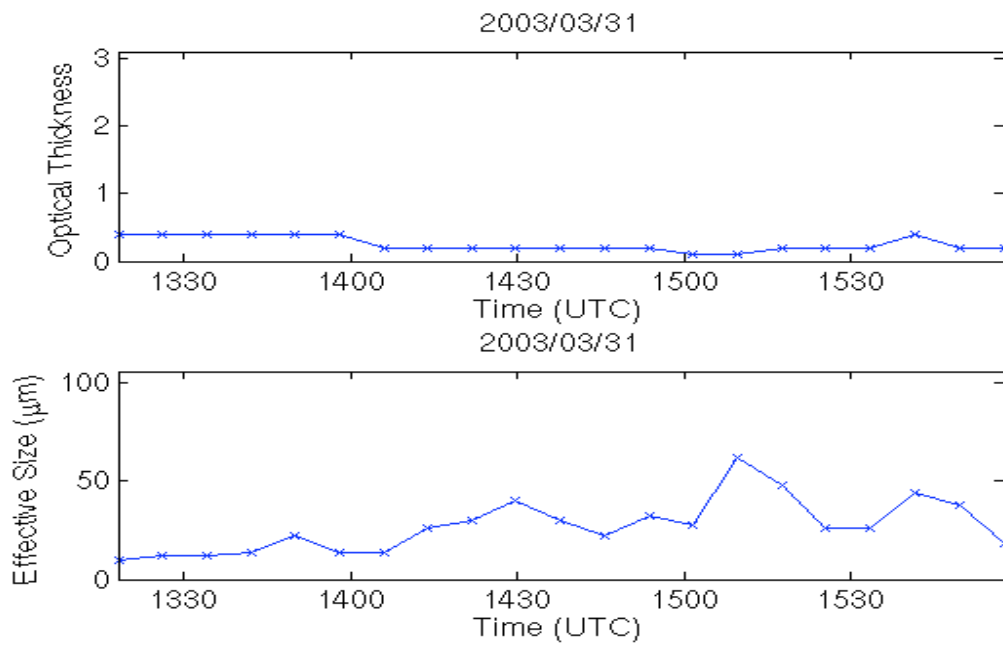


FIG. 24. Retrieved optical thickness (top) and effective size (bottom) for 03/31/2003.

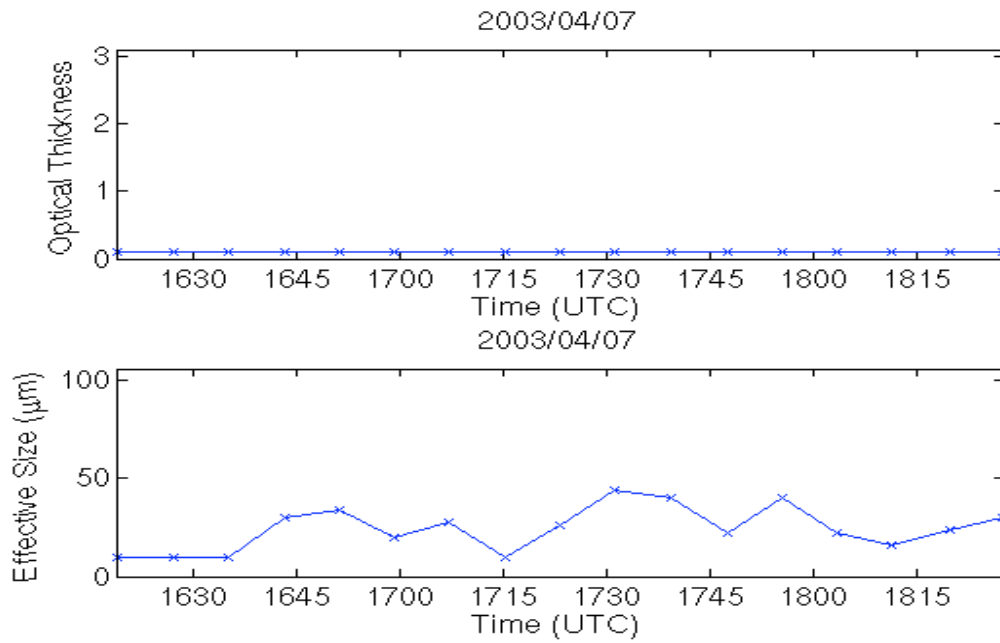


FIG. 25. Retrieved optical thickness (top) and effective size (bottom) for 04/07/2003.

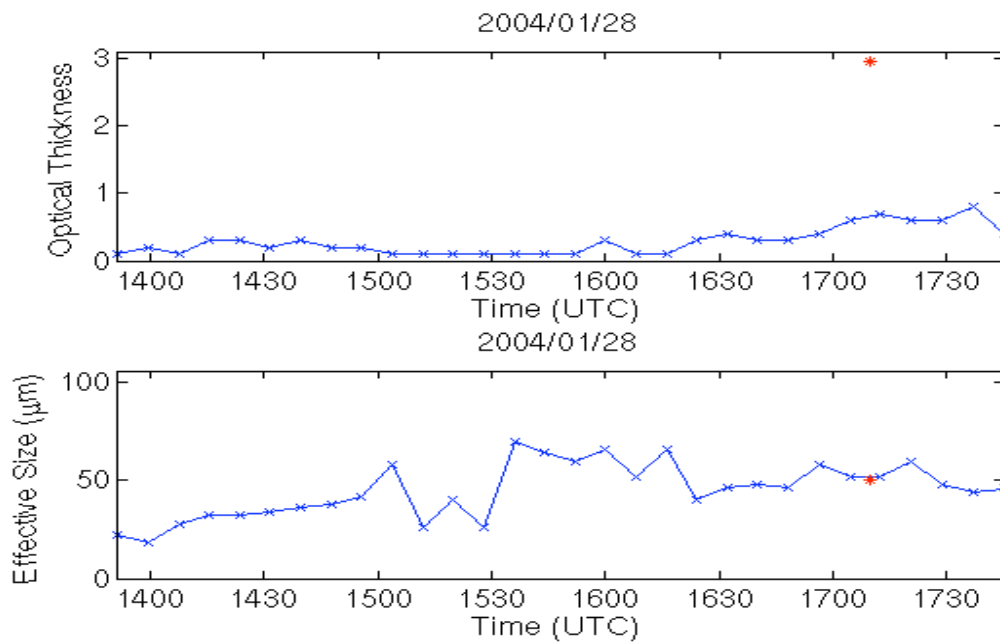


FIG. 26. Retrieved optical thickness (top) and effective size (bottom) for 01/28/2004. MODIS retrieved optical thickness and effective size are denoted by a (*).

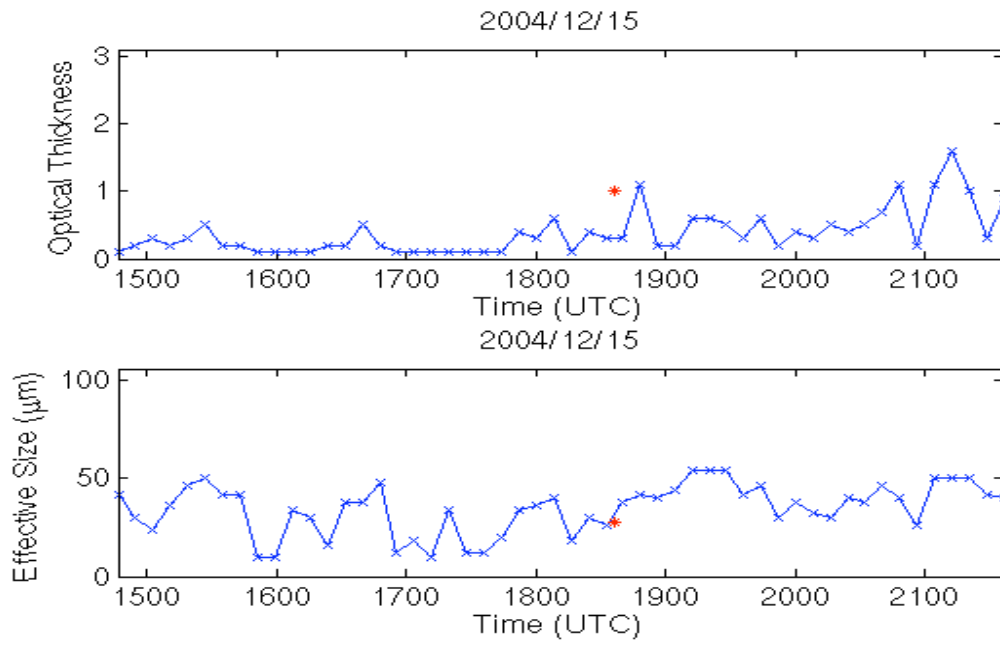


FIG. 27. Retrieved optical thickness (top) and effective size (bottom) for 12/15/2004. MODIS optical thickness and effective size are denoted by a (*).

b. North Slope of Alaska (NSA)

Five cases were selected for the NSA region. MODIS validation was unable to be completed for any of the NSA cases because all but one case occurred during the winter, and Barrow, Alaska never gets full daylight during the winter. Selection of cases for this region was difficult because of a lack of sounding and AERI data. The soundings were only done once a day, and many days are missing data. There are also many time periods missing AERI data. There was also some persistence of low-level clouds, especially during the summer. These two things significantly limited our selection of cases to choose from.

The cloud information is listed in Table 4. As before it is assumed that the clouds are composed mostly of ice crystals. This is reasonable because the warmest cloud base temperature is 243.150 K.

TABLE 4. NSA cloud cases.

Date	Time Period (UTC)	Cloud Base Height (km) (hPa)	Cloud Base Temperature (K)
11/06/2002	0815 – 1705	7.54 (359.2)	225.350
11/07/2002	0805 – 1115	10.0 (245.9)	221.050
11/25/2002	1555 – 1850	5.37 (497.1)	243.150
01/29/2003	0930 – 1610	5.78 (467.3)	236.55
05/07/2003	1235 – 1520	5.5 (494.4)	228.450

Figures 28 - 32 show the MPL-measured cloud base heights for each case, and Figs. 33 - 37 show the retrieved values of optical thickness and effective size. Looking at the cloud base heights we see that they are quite scattered for this region. As in the daytime cases at the SGP region, this made it more difficult to accurately retrieve the cloud base height.

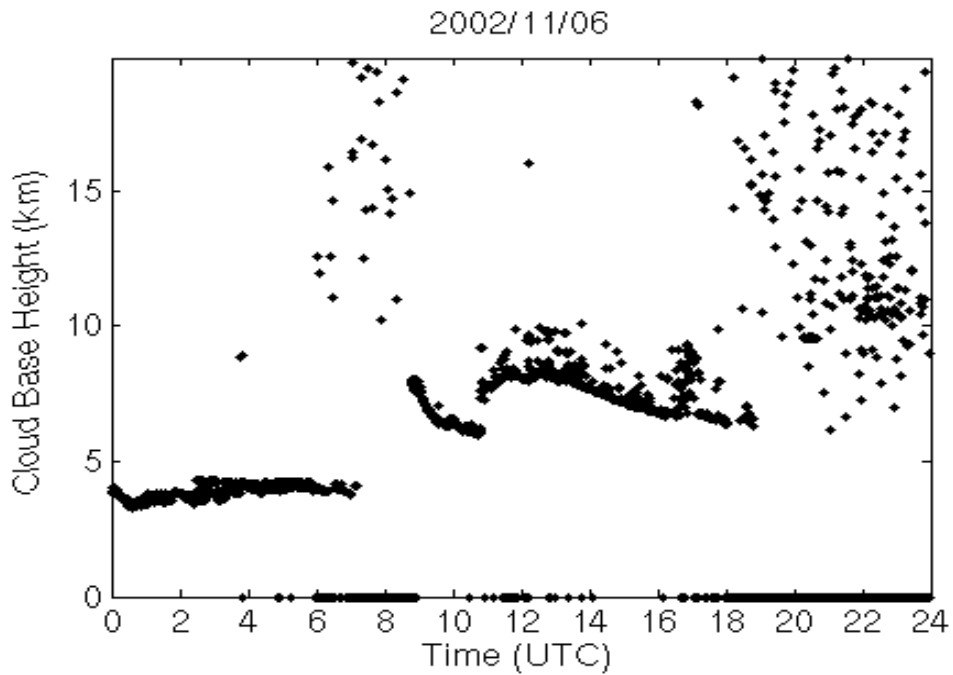


FIG. 28. MPL-calculated cloud base height for 11/06/2002 at NSA.

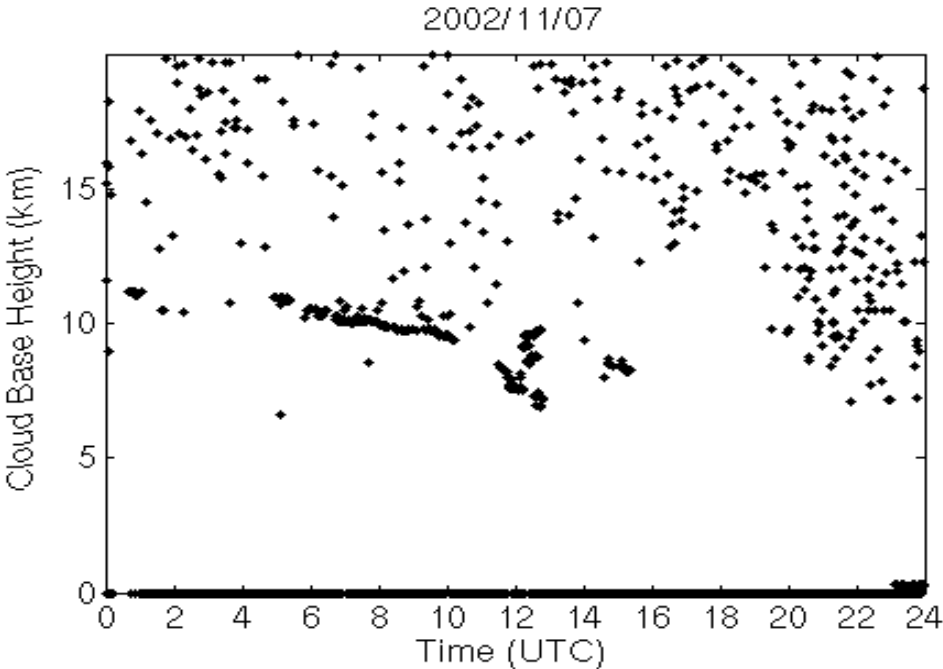


FIG. 29. MPL-measured cloud base height for 11/07/2002 at NSA.

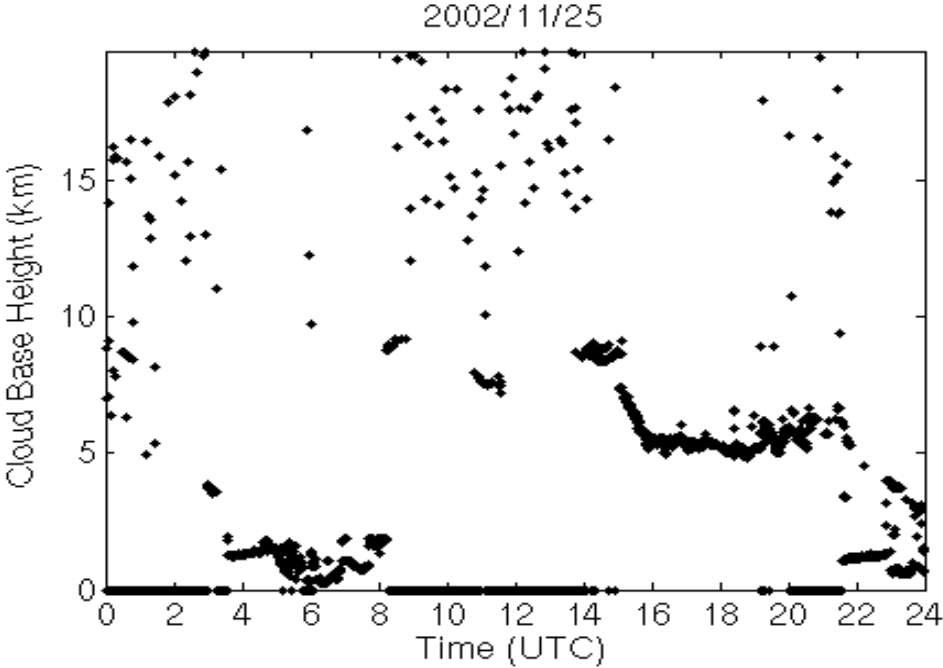


FIG. 30. MPL-calculated cloud base height for 11/25/2002 at NSA.

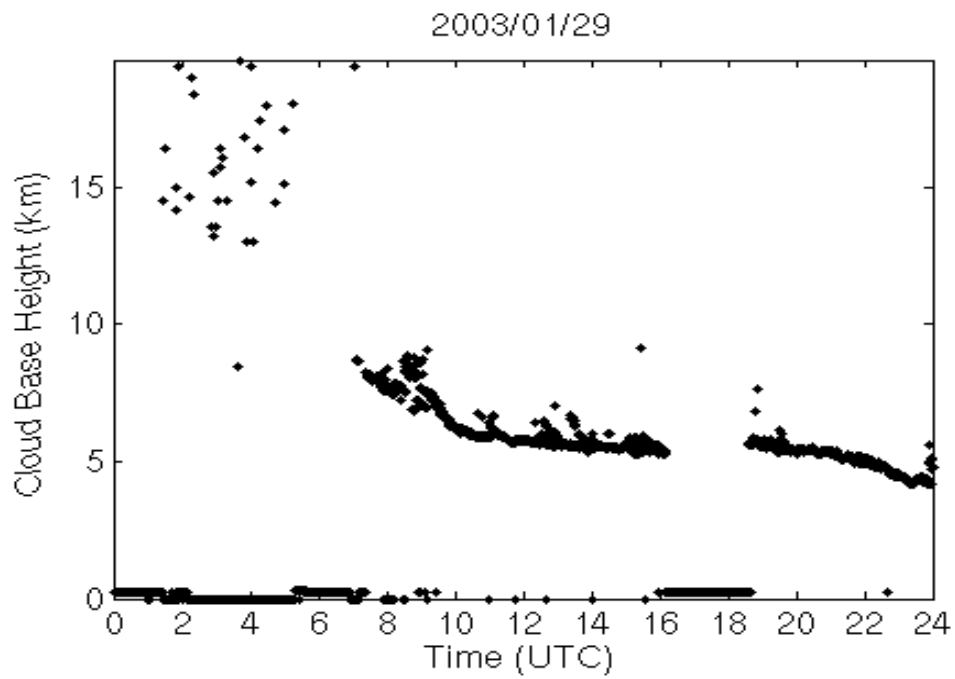


FIG. 31. MPL-calculated cloud base height for 01/29/2003 at NSA.

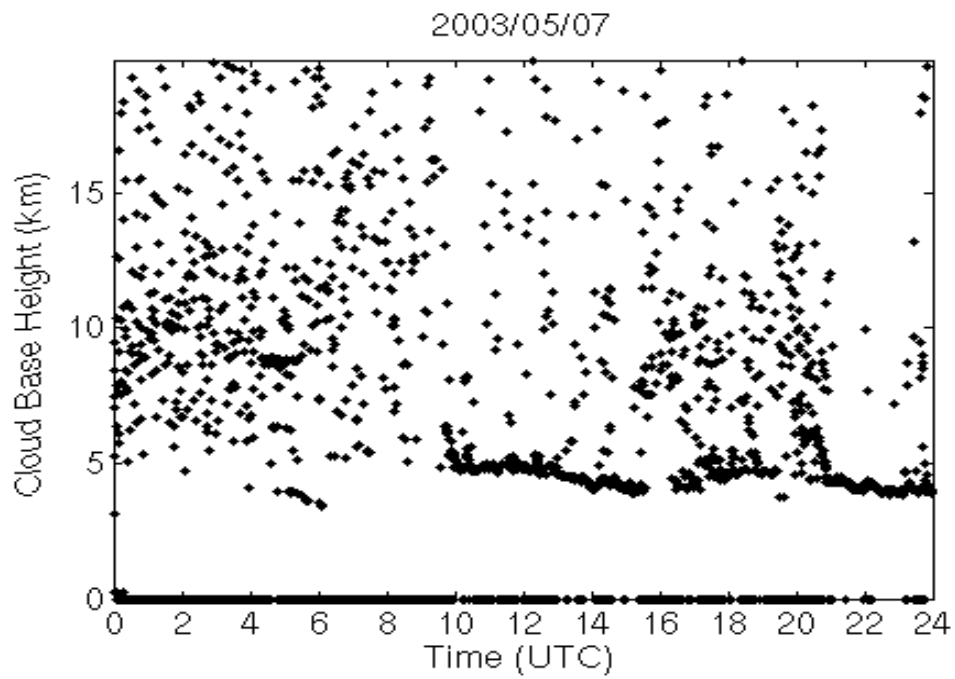


FIG. 32. MPL-calculated cloud base height for 05/07/2003 at NSA.

Now we can look at our retrieved values of optical thickness and effective size for this region. On November 6, 2002 the optical thickness was pretty steady. It ranged from 0.1 to 0.8 with a mean of 0.42. The effective size was more unsteady than the optical thickness, although it had a general increase over the time period examined. It ranged from 12 to 88 μm with a mean of 53.2 μm . On November 7, 2002 the optical thickness had a sharp increase around 0900 UTC, but other than that it remained reasonably steady. Over the time period examined it ranged from 0.2 to 1.8 and had a mean of 0.58. The effective size was a little more constant and ranged from 14 to 52 μm with a mean of 36.8 μm . There is no jump in effective size corresponding to the jump in optical thickness. On November 25, 2002 the optical thickness was very unsteady but did have a general decreasing trend. Its range was from 0.1 to 2 with a mean of 0.713. The effective size for this case was very steady and only ranged from 46-80 μm with a mean of 56.3 μm . Next, on January 29, 2003 the optical thickness was steady with an increase towards the end of the time period. It ranged from 0.1 to 0.9 with a mean of 0.37. The effective size was very unsteady, jumping everywhere. It ranged from 24 to 106 μm with a mean of 62.3 μm . Finally, on May 7, 2003, the optical thickness ranged from 0.1 to 0.5 with a mean of 0.22. The effective size was the most unstable of all the cases, ranging from 10 to 106 μm with a mean of 66.43 μm . These retrieved values are comparable to the values retrieved for the night cases at the SGP.

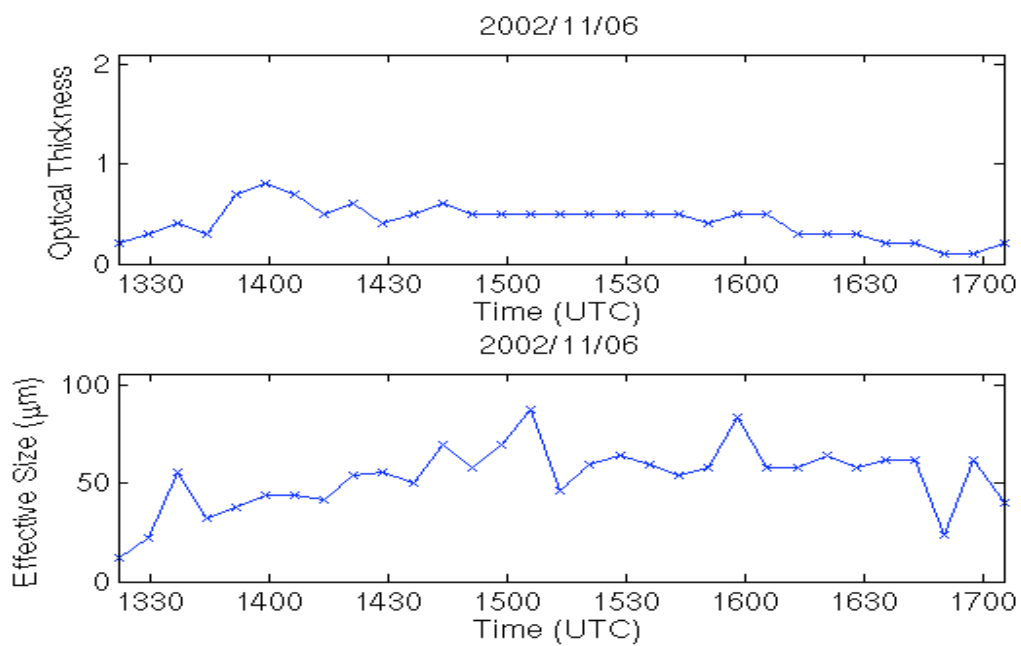


FIG. 33. Retrieved optical thickness (top) and effective size (bottom) for 11/06/2002.

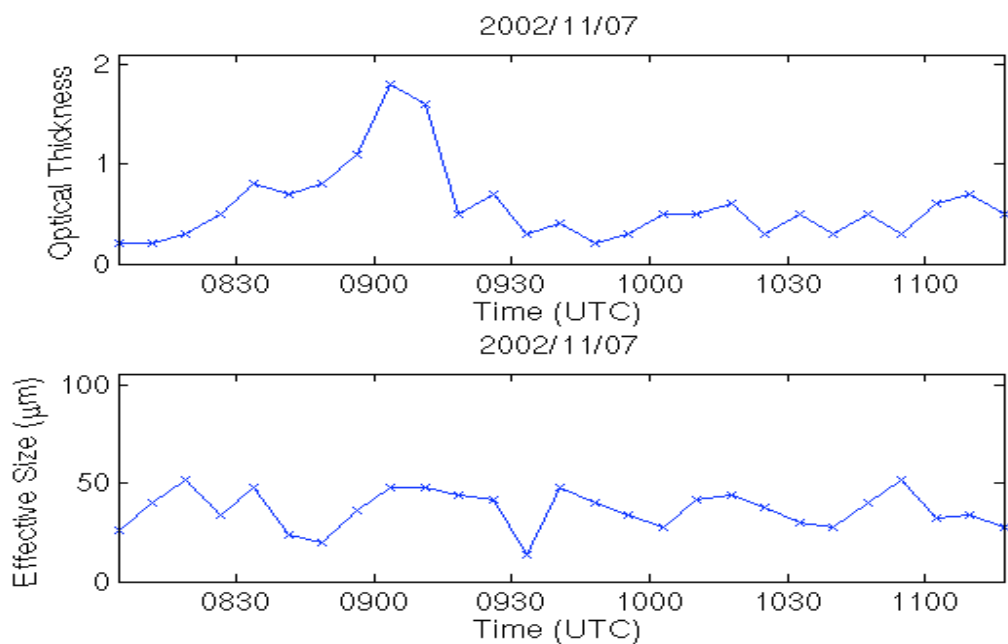


FIG. 34. Retrieved optical thickness (top) and effective size (bottom) for 11/07/2002.

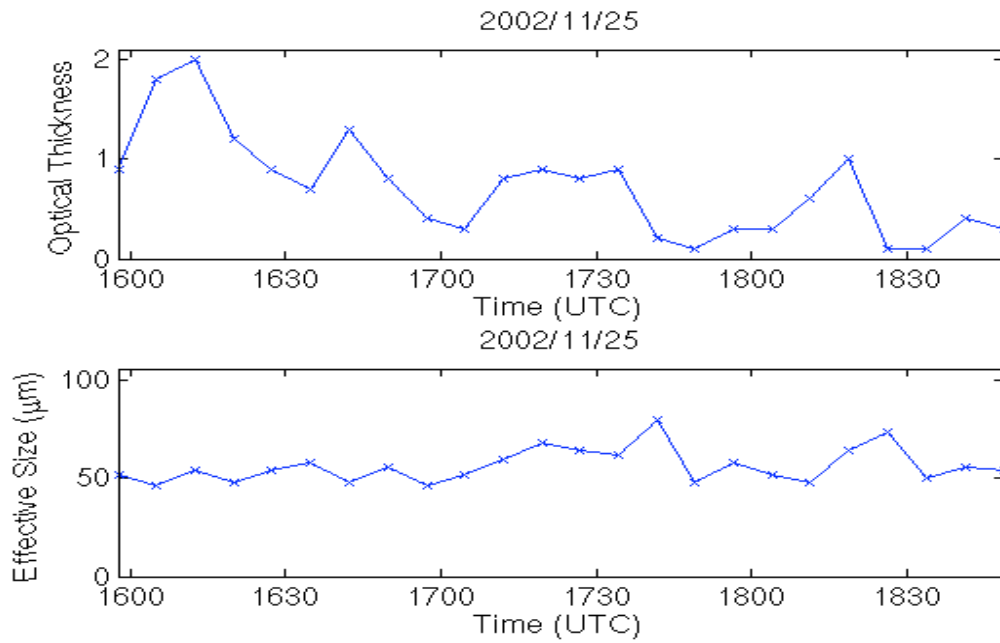


FIG. 35. Retrieved optical thickness (top) and effective size (bottom) for 11/25/2002.

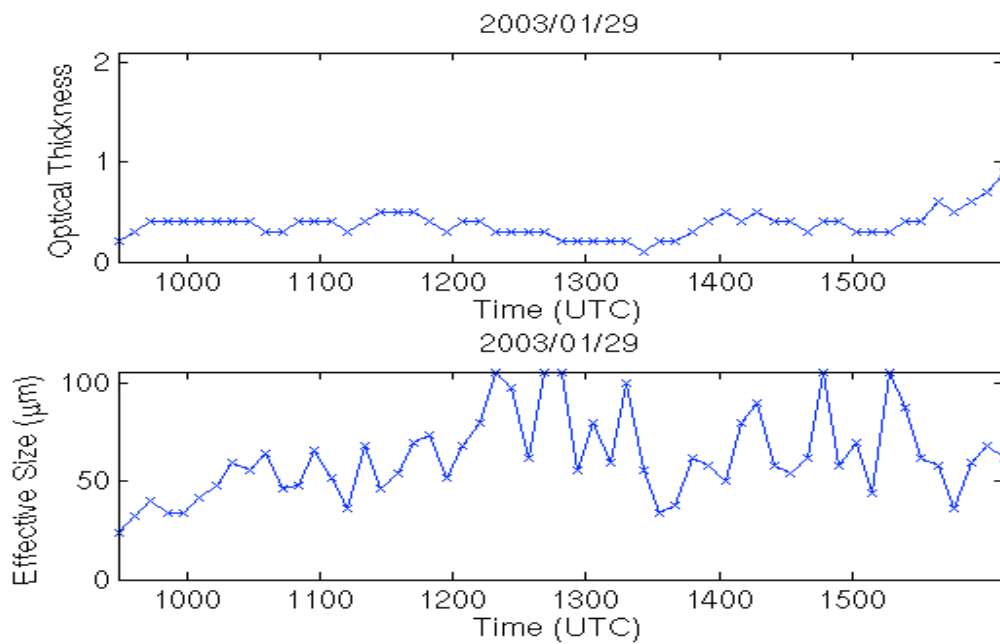


FIG. 36. Retrieved optical thickness (top) and effective size (bottom) for 01/29/2003.

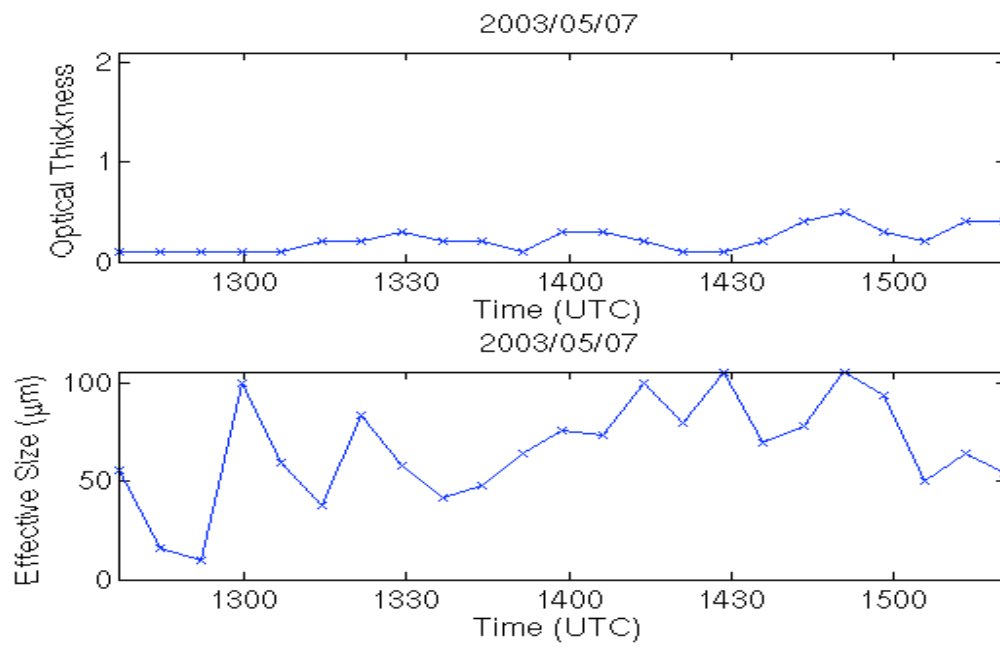


FIG. 37. Retrieved optical thickness (top) and effective size (bottom) for 05/07/2003.

6. CONCLUSIONS

Cirrus clouds have a significant impact on the earth's radiation energy budget, but they are still one of the least understood components of climate research. The radiative and microphysical properties of clouds must be determined to improve the accuracy and reliability of numerical weather prediction and general climate models. Many methods have been introduced to attempt to retrieve the optical and microphysical properties of cirrus clouds using radiation measurements in the infrared region.

The research presented in this thesis applied the retrieval technique developed by Yang *et al.* (2005a) to simultaneously retrieve the optical thickness and particle effective size of ice clouds. This study focused on single-layer ice clouds in the midlatitude and polar regions using data from the ARM field campaign. Guo *et al.* (2005) did a similar study focusing on the tropical region using data from the CRYSTAL-FACE field campaign.

A fast model was developed for this study. It is based on the AIRS clear-sky model (Strow *et al.*, 2003) and the corresponding for radiative transfer in a cloudy atmosphere (Wei *et al.*, 2004). This model assumes that clouds are located in a plane-parallel, single homogeneous, and isothermal layer.

The gamma technique introduced by Smith *et al.* (1993) was used to reduce errors in the retrieval algorithm. The technique involved matching the measured and calculated clear-sky radiances by adjusting the calculated transmittance profile. The gamma technique was very successful in matching these two radiance profiles. After the

gamma adjustment, the error between the measured and calculated clear-sky radiance generally remained under 5%.

Overall, the retrieval method examined in this study seems to perform well. Due to the data constraints and some persistent low-level clouds, it performed much better in the mid-latitude regions than the polar regions. There were more limitations on cases in the polar region than the midlatitude. This meant there were less cases available to examine in the polar region than the midlatitude. The retrieval method could be improved by making the model able to calculate the radiance for multiple cloud layers. Being able to account for some low-level clouds would greatly increase the number of cases available.

Our values for effective size at the SGP region agree moderately well with the MODIS values, except in the 2003 case where our effective size greatly underestimated the MODIS effective size. The retrieval of the effective size seems to be highly variable. Presumably this is because the radiance profile is less sensitive to changes in effective size than changes in optical thickness (as can be seen in Fig. 5).

Our values for optical thickness at the SGP region were always significantly less than the MODIS values. The optical thickness retrieval seems to be biased towards smaller values during the day. More investigation needs to be completed to determine the causes of these discrepancies.

REFERENCES

- Auer, A. H., D. L. Veal, 1970: The Dimension of Ice Crystals in Natural Clouds. *J. Atmos. Sci.*, **27**, 919-926.
- Chandrasekhar, S., 1960: *Radiative Transfer*, Dover, 393.
- Collard, A. D., S. A. Ackerman, W.L. Smith, X. Ma, H. E. Revercomb, R. O. Knuteson, and S-C. Lee, 1995: Cirrus Cloud Properties Derived from High Spectral Resolution Infrared Spectrometry During FIRE II. Part III: Ground-Based HIS Results. *J. Atmos. Sci.*, **52**, 4264-4275.
- DeSlover, D. H. and W. L. Smith, 1999: A Methodology for Measuring Cirrus Cloud Visible-to-Infrared Spectral Optical Depth Ratios. *J. Atmos. and Oceanic Tech.*, **16**, 251-262.
- Foot, J. S., 1988: Some Observations of the Optical Properties of Clouds. Part II: Cirrus. *Quart. J. Roy. Met. Soc.*, **114**, 145-164.
- Francis, P. N., A. Jones, R. W. Saunders, K. P. Shine, A. Slingo, Z. Sun, 1994: An Observational and Theoretical Study of the Radiative Properties of Cirrus: Some Results from ICE'89. *Quart. J. Roy. Met. Soc.*, **120**, 809-848.
- Fu, Q., P. Yang, W. B. Sun, 1998: An Accurate Parameterization of the Infrared Radiative Properties of Cirrus Clouds for Climate Models. *J. Climate*, **11**, 2223-2237.
- Grenfell, T. C., S. G. Warren, 1999: Representation of Nonspherical Ice Particles by a Collection of Independent Spheres for Scattering and Absorption of Radiation. *J. Geophys. Research*, **104**, 31697-31709.
- Guo, G., Q. Ji, P. Yang, S-C. Tsay, 2005: Remote Sensing of Cirrus Optical and Microphysical Properties From Ground-Based Infrared Radiometric Measurements. Part II: Retrievals From CRYSTAL-FACE Measurements. *IEEE Geosci. and Remote Sens. Letters*, **2**, 132-135.
- Heidinger, A., 1998: Nadir sounding of clouds and aerosols in the Q2 A-band. Ph.D. dissertation, Colorado State University, 226 pp. [Available from Colorado State University, Department of Atmospheric Sciences, Fort Collins, CO 80523]
- Huang, H-L., P. Yang, H. Wei, B. A. Baum, Y. Hu, P. Antonelli, S. A. Ackerman, 2004: Inference of Ice Cloud Properties from High Spectral Resolution Infrared Observations. *IEEE Tran. Geosci. and Remote Sens.*, **42**, 842-853.

- King, M. D., W. P. Menzel, Y. J. Kaufman, D. Tanre, B-C. Gao, S. Platnick, S. A. Ackerman, L. A. Remer, R. Pincus, P. A. Hubanks, 2003: Cloud and Aerosol Properties, Precipitable Water, and Profiles of Temperature and Water Vapor from MODIS. *IEEE Trans. on Geosci. and Remote Sens.*, **41**, 442-458
- Liou, K-N., 1986: Influence of Cirrus Clouds on Weather and Climate Processes: A Global Perspective. *Monthly Weather Review.*, **114**, 1167-1199.
- _____, K. N., 2002: *An Introduction to Atmospheric Radiation*, Academic Press, 583.
- Lynch, D. K., K. Sassen, D. O. Starr, and G. Stephens, 2002: *Cirrus*, Oxford University Press, 480.
- Ono, A., 1969: The Shape and Riming Properties of Ice Crystals in Natural Clouds. *J. Atmos. Sci.*, **27**, 138-147.
- Platnick, S., M. D. King, S. A. Ackerman, W. P. Menzel, B. A. Baum, J. C. Riedi, R. A. Frey, 2003: The MODIS Cloud Products: Algorithms and Examples from Terra. *IEEE Trans. on Geosci. and Remote Sens.*, **41**, 459-473.
- Rothman, L. S., A. Barbe, D. C. Benner, L. R. Brown, C. Camy-Peyret, M. R. Carleer, K. Chance, C. Clerbaux, V. Dana, V. M. Devi, A. Fayt, J-M. Flaud, R. R. Gamache, A. Goldman, D. Jacquemart, K. W. Jucks, W. J. Lafferty, J-Y. Mandin, S. T. Massie, W. Nemtchinov, D. A. Newnham, A. Perrin, C. P. Rinsland, J. Shroeder, K. M. Smith, M. A. H. Smith, K. Tang, R. A. Toth, J. V. Auwera, P. Varanasi, K. Yoshino, 2003: The HITRAN Molecular Spectroscopic Database: Edition of 2000 Including Updates Through 2001. *J. Quant. Spect. Rad. Trans.*, **82**, 5-44.
- Smith, W. L., X. L. Ma, S. A. Ackerman, H. E. Revercomb, and R. O. Knuteson, 1993: Remote Sensing Cloud Properties from High Spectral Resolution Infrared Observations. *J. Atmos. Sci.*, **50**, 1708-1720.
- _____, W. L., H. E. Revercomb, R. O. Knuteson, F. A. Best, R. Dedecker, H. B. Howell, and H. M. Woolf, 1995: Cirrus Cloud Properties Derived from High Spectral Resolution Infrared Spectrometry During FIRE II. Part I: The High Resolution Interferometer Sounder (HIS) Systems. *J. Atmos. Sci.*, **52**, 4238-4245.
- Stamnes, K., S-C. Tsay, W. Wiscombe, K. Jayaweera, 1988: Numerically Stable Algorithm for Discrete-Ordinate-Method Radiative Transfer in Multiple Scattering and Emitting Layered Media. *Applied Optics*, **27**, 2502-2509.

- Stephens, G. L., S-C. Tsay, P. W. Stackhouse, and P. J. Flatau, 1990: The Relevance of the Microphysical and Radiative Properties of Cirrus Clouds to Climate and Climatic Feedback. *J. Atmos. Sci.*, **47**, 1742-1753.
- Strow, L.L. S. E. Hannon, S. De Souza-Machado, H. E. Motteler, D. Tobin, 2003: An Overview of the AIRS Radiative Transfer Model. *IEEE Trans. Geosci. Remote Sensing*, **41**, 303-313.
- Wei, H., P. Yang, J. Li, B. A. Baum, H-L. Huang, S. Platnick, Y. Hu, and L. Strow, 2004: Retrieval of Semitransparent Ice Cloud Optical Thickness From Atmospheric Infrared Sounder (AIRS) Measurements. *IEEE Trans. Geosci. Remote Sens.*, **42**, 2254-2267.
- Yang, P. and K. N. Liou, 1996a: Finite-Difference Time Domain Method for Light Scattering by Small Ice Crystals in Three-dimensional Space. *J. Opt. Soc. Amer.*, **A13**, 2072-2085.
- _____, and _____, 1996b: Geometric-Optics-Integral-Equation Method for Light Scattering by Nonspherical Ice Crystals. *Appl. Opt.*, **35**, 6568-6584.
- _____, B-C. Gao, B. A. Baum, Y. X. Hu, W. J. Wiscombe, S-C. Tsay, D. M. Winker, and S. L. Nasiri, 2001: Radiative Properties of Cirrus Clouds in the Infrared (8-13 mm) Spectral Region. *J. Quant. Spect. & Rad. Trans.*, **70**, 473-504.
- _____, S-C. Tsay, H. Wei, G. Guo, and Q. Ji, 2005a: Remote Sensing of Cirrus Optical and Microphysical Properties from Ground-Based Infrared Radiometric Measurements. Part I: A New Retrieval Method Based on Microwindow Spectral Signature. *IEEE Geosci. and Remote Sens. Letters*, **2**, 128-131.
- _____, H. Wei, H-L. Huang, B. A. Baum, Y. X. Hu, G. W. Kattawar, M. I. Mishchenko, and Q. Fu, 2005b: Scattering and Absorption Property Database for Nonspherical Ice Particles in the Near-Through Far-Infrared Spectral Region. *Appl. Opt.* Accepted
- Yee, K. S., 1966: Numerical Solution of Initial Boundary Problems Involving Maxwell's Equations in Isotropic Media. *IEEE Trans. Antennas Propagat*, **14**, 302-307.

VITA

Biography

Jacqueline Anne Kinney was born in Dallas, TX, on February 3, 1981. She lived in Dallas her whole childhood. She graduated from Richardson High School in May of 1999 and enrolled in Texas A&M University as a freshman the following fall. Her permanent address is 8603 Cretys Cove, Austin, TX 78745.

Educational Background

B.S., Meteorology, Texas A&M University, May 2003.

M.S., Atmospheric Sciences, Texas A&M University, August 2005.

Publications

Evans, E., N. Bahatti, J. Kinney, L. Pann, M. Pena, S-C Yang, E. Kalnay, and J. Hansen, 2004: RISE Undergraduates Find that Regime Changes in Lorenz's Model are Predictable, *Bulletin of the American Meteorological Society*, **85**, 520-524.